AD-A146 967 DEVELOPMENT OF A NAVIER-STOKES ROTOR/STATOR ANALYSIS 1/1
(U) SCIENTIFIC RESEARCH ASSOCIATES INC GLASTONBURY CT
S J SHAMROTH ET AL. JUN 84 SRA-R84-910004-1
UNCLASSIFIED AFOSR-TR-84-0858 F49620-83-C-0119 F/G 20/4 NL

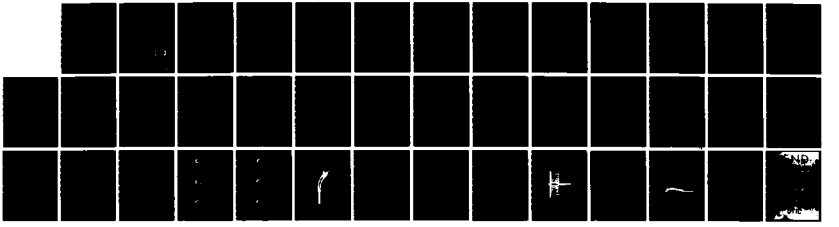

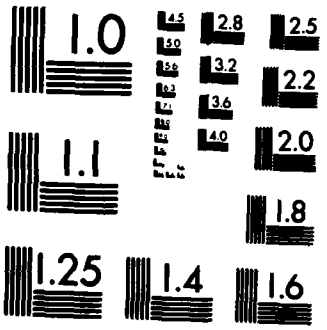
1.0
1.1
1.25
1.4
1.6
1.8
2.0
2.2
2.5
2.8
3.2
3.6
4.0
4.5
5.0

AFOSR-TR- 84-0858

(3)

R84-910004-1

DEVELOPMENT OF A NAVIER-STOKES ROTOR/STATOR ANALYSIS

S.J. Shamroth, H. McDonald, B.C. Weinberg, D.V. Roscoe
Scientific Research Associates, Inc.
P.O. Box 498
Glastonbury, CT 06033

June 1984

Prepared for:
Air Force Office of Scientific Research

UNCLASSIFIED

SECURITY CLASSIFICATION OF THIS PAGE (When Data Entered)

REPORT DOCUMENTATION PAGE	READ INSTRUCTIONS BEFORE COMPLETING FORM
1. REPORT NUMBER: AFOSR-TR- 84-0858	2. GOVT ACCESSION NO. / 3. RECIPIENT'S CATALOG NUMBER
4. TITLE (and Subtitle): Development of a Navier-Stokes Rotor/Stator Analysis	5. TYPE OF REPORT & PERIOD COVERED: 21 June 83 - 30 June 84
	6. PERFORMING ORG. REPORT NUMBER: R84-910004-1
7. AUTHOR(s): S. J. Shamroth, H. McDonald, B. C. Weinberg, D. V. Roscoe	8. CONTRACT OR GRANT NUMBER(s): F49620-83-C-0119
9. PERFORMING ORGANIZATION NAME AND ADDRESS: SCIENTIFIC RESEARCH ASSOCIATES, INC. P.O. BOX 498 GLASTONBURY, CT 06033	10. PROGRAM ELEMENT, PROJECT, TASK AREA & WORK UNIT NUMBERS: 61102F 2307 /A4
11. CONTROLLING OFFICE NAME AND ADDRESS: AIR FORCE OFFICE OF SCIENTIFIC RESEARCH/NA BOLLING AFB, DC 20332	12. REPORT DATE: June 1984
	13. NUMBER OF PAGES: 39
14. MONITORING AGENCY NAME & ADDRESS (if different from Controlling Office)	15. SECURITY CLASS. (of this report): Unclassified
	15a. DECLASSIFICATION/DOWNGRADING SCHEDULE

16. DISTRIBUTION STATEMENT (of this Report)

Approved for public release; distribution unlimited

17. DISTRIBUTION STATEMENT (of the abstract entered in Block 20, if different from Report)

18. SUPPLEMENTARY NOTES

19. KEY WORDS (Continue on reverse side if necessary and identify by block number)

Navier-Stokes Equations
Rotor-Stator Analysis
Unsteady Flow

20. ABSTRACT (Continue on reverse side if necessary and identify by block number)

An important problem in axial flow turbomachinery is that of flow through a turbine or compressor stage in which interaction occurs between the rotor and the stator. Although several experimental efforts have focused upon this problem, relatively little analysis has been applied to this problem. The present effort applies a Navier-Stokes analysis to the rotor/stator problem. The effort consists of several tasks. These include assessment of an existing Navier-Stokes analysis for time-dependent flows, exploration of appropriate boundary conditions, development of an appropriate coordinate system and a demonstration —(over)—

DD FORM 1 JAN 73 1473 EDITION OF 1 NOV 65 IS OBSOLETE

UNCLASSIFIED

SECURITY CLASSIFICATION OF THIS PAGE (When Data Entered)

calculation. The present annual report discusses the time-dependent assessment, exploration of boundary conditions and the coordinate system problem.

TABLE OF CONTENTS

INTRODUCTION

In both the compressor and turbine the interaction of the rotor with the stator is critical to the function of the stage. In the rotor work is either performed on or extracted from the gas and in the stator a rotational component either removed or imparted to the flow. In view of the relative motion of the rotor to the stator, the basic interaction is unsteady in nature. In recent years there has been conflicting evidence on the effect of spacing on stage performance. Here spacing refers to the distance between the trailing edge and the leading edge, or vice versa. Obviously there are profound beneficial structural effects which follow from having a short spacing distance. The overall machine is shorter, bearings have lower steady loads and main shafts can be shorter and stronger for a given weight. As might be expected, moving the rotor and stator closer together can result in a very strong, complex aerodynamic interaction. Moving the rotor and stator further apart might be expected to reduce the transient aerodynamic loads involved, a beneficial effect obtained at a very significant cost. However, the complexity of the rotor-stator interaction has resulted in conflicting experimental evidence on the effect of spacing. The complexity of the interaction is significantly greater in modern highly loaded or high work stages operating in the transonic regime. The indications are that the complex interaction between the stator and the rotor is not as well understood as would be desired. An improved understanding could clearly have a pronounced beneficial effect on stage performance and durability.

In a series of AFOSR-sponsored programs, Detroit Diesel Allison has studied experimentally various aspects of the unsteady flow in a compressor (Ref. 1,2,3,4) and made comparisons with inviscid theories of varying degrees of complexity. While very encouraging, much remains to be done, particularly since inviscid theories cannot treat vorticity production effects. Another experimental effort focusing upon the interaction problem is that of Dring, Joslyn, Hardin and Wagner (Ref. 5) who investigated the effect of gap on and in the interaction process. These experiments clearly show the importance of understanding the effect of rotor-stator gap spacing and an understanding of the basic fluid mechanics involved in this problem would be a major aid to the research and development engineer.

In developing an analysis to predict the stator-rotor flow field, it is clear that viscous effects must be included. The work under the present effort attacks this problem by applying a time-dependent Navier-Stokes analysis to the stator-rotor flow field. The analysis has been successfully used for calculating the flow about a variety of cascade configurations (e.g. Refs. 6-10). Under the present effort, the transient accuracy of the Navier-Stokes code would be assessed, possible radiative boundary condition formulations included, a stator-rotor grid developed and a demonstration case run.

ACTIVITY DURING THE PAST YEAR

Transient Accuracy

Although the Navier-Stokes code had been well exercised, most of the effort had focused upon calculation for flow in steady configurations. In order to apply the code to the stator-rotor problem, a time-dependent application is required. Therefore, the first task in the program was to obtain an assessment of the time-dependent accuracy of the code. In this regard, two calculations were considered. The first was done under contract to NASA-Langley Research Center as part of a dynamic stall analysis and since it is relevant to the present effort, the results will be presented here. The full details of the case can be found in Ref. 11. The case considered is that of an NACA 0012 airfoil oscillating sinusoidally in pitch in a stream with a Reynolds number based on chord of 2.08×10^6 and a Mach number of 0.30. The airfoil oscillated between 4° and 20° with a dimensionless frequency of 0.125. The case corresponds to Data RUN 51.005 of the data of St. Hilaire and Carta (Refs. 12 and 13). Although this calculation represents an isolated airofil rather than a cascade, it was made with the cascade deck with boundary conditions appropriate to the isolated airfoil applied.

Comparisons between calculated and measured surface pressure coefficients are shown in Figs. 1-8. three comparisons during the upstroke are shown in Figs. 1 and 2. As can be seen, the agreement is good. The data was reconstructed from the Fourier coefficient given by St. Hilaire and Carta (NASA CR-165927). The third measured data point on the pressure surface ($x/c \approx .066$) gave very erratic results and was not plotted for most of the

comparisons. The excellent comparisons shown in Figs. 1 and 2 give evidence to the time-accurate calculation for the surface pressure.

Figure 3 presents a comparison at $\alpha = 17.7°$, $\alpha > 0$. This is near the incidence where stall would first be inferred from the lift and moment curves. The figure shows some discrepancy between predicted and measured values as the data presents some evidence of a vortex being shed on the suction surface leading edge. The discrepancy increases in Fig. 4 where the data clearly indicates stall. The calculated plateau on the suction surface, $x/c \approx .15$, seems to indicate a vortex being initiated. Furthermore, the calculated maximum suction peak at $\alpha = 19.5°$, Fig. 4, is considerably less than that at $\alpha = 17.7°$, Fig. 3. Based upon the plateau and the drop in suction peak the calculated distribution at 19.5° appears to be beginning the stall process. The data at 19.5° is presented with the calculation at $\alpha = 19.9°$, $\dot{\alpha} > 0$ in Fig. 5. Although these are at different values of α, they represent pressure distributions at approximately the same incremental time after stall is initiated; the distributions are remarkably similar. Comparisons over the downstroke are given in Figs. 6-8. Obviously, the basic trends are in agreement as a strong qualitative comparison is shown between the calculation and the measured data. The results of this calculation particularly prior to stall, Figs. 1-3, indicate the time-accuracy of the procedure at least as far as surface pressure is concerned.

The second case considered was performed under the present effort. The case was a 25.5% thick Joukowski airfoil entering a gust in which the vertical velocity is 0.25 times the freestream velocity. This case was also calculated by Giesing via an inviscid analysis (Ref. 14) and although viscous effects are present in the present analysis, it is expected that the calculated pressure gradients should be in reasonable agreement if little or no separation occurs. Calculated surface pressure distributions from both techniques are presented in Figs. 9-12 where T indicates the location of the gust relative to the airfoil leading edge. As can be seen, the two calculations are in good agreement. The major discrepancies are the appearance of surface pressure discontinuities in the inviscid solution which are not found in the viscous solution such as at $x/c = .25$ in Fig. 10. However, this is the expected result of viscous effects. Contour plots of pressure coefficient are presented in Figs. 13 and 14, where it can be seen that initially, the pressure coefficient is nearly symmetric, but by $T = -.10$ it has become distinctly asymmetric. It should be noted that at $T = -.10$ the

center of the gust is at x/c = -.10, however, due to viscous effects the gust front is not a sharp line but diffuses over a finite region. Therefore, some effect is felt at T = -.10. Velocity vector plots are given in Figs. 15 and 16. This comparison along with the dynamic stall calculations of Ref. 11 serve to confirm the time-accuracy capability of the cascade code.

Boundary Conditions

Previous experience in solving Navier-Stokes equations has indicated the important role boundary conditions play in obtaining accurate solutions and rapid numerical convergence. Improper specification and/or implementation of boundary conditions can lead to problems in achieving convergence and solution accuracy for the solution procedure. In order to set a framework for the discussion to follow, it is useful to review the manner in which boundary conditions are set for calculations in which a steady state solution is sought. In these steady state solution cases, the Navier-Stokes cascade analysis followed the suggestion of Briley and McDonald (Ref. 15) which specifies upstream total pressure and downstream static pressure conditions. For the cascade system shown in Fig. 17, *AB* and *CD* are periodic boundaries and periodic conditions are set here.

Specification of upstream and downstream conditions is somewhat more difficult. For an isolated cascade, boundary conditions for the differential equations may be known at both upstream infinity and downstream infinity. However, since computation economics argues for placing grid points in the vicinity of the cascade and minimizing the number of grid points far from the cascade, the upstream and downstream computational boundaries should be set as close to the cascade as is practical. However, when the upsteam boundary is placed close to the cascade upstream influence of the cascade modifies the flow such that far field function boundary conditions may be inappropriate.

In the approach used to date, the suggestion of Ref. 15 is followed which sets total pressure on boundary BC (see Fig. 17). Unless boundary BC is very far upstream, the flow velocity along this boundary will not be equal to the velocty at upstream infinity since some inviscid deceleration will have occurred. However, as long as the boundary is upstream of the region of any significant viscous or shock phenomena, the total pressure on this boundary will be equal to the total pressure at upstream infinity. Hence,

total pressure is an appropriate boundary condition realistically modeling the desired flow condition. In addition to specifying upstream total pressure, it is necessary to specify the inlet flow angle. In the present calculation, a specified constant angle was assumed on the upstream boundary. The upstream boundary condition specification was completed by setting the first derivative of density to zero. The downstream boundary was treated by setting a constant static pressure as a boundary condition, and by setting second derivatives of both velocity components equal to zero at this location. In the present application, a constant static pressure was set at downstream infinity. Implicit in this assumption is that the downstream boundary is located in a region where pressure is uniform in the transverse direction although a nonuniform specification is permitted numerically and possible physically. The final boundary conditions to be considered are the conditions along the blade surface. Here no-slip and no through-flow conditions were applied leading to a specification of zero velocity on the surface. An inviscid transverse momentum equation was applied on the surface leading to a boundary condition approximation of zero transverse pressure gradient being applied.

The second item which must be considered in regard to boundary conditions is their implementation. Both the upstream and downstream boundaries have boundary conditions associated with them which are nonlinear functions of the dependent variables. These are the specifications of total pressure on the upstream boundary and static pressure on the downstream boundary. These nonlinear boundary conditions are linearized in the same manner as the governing equations, via a Taylor expansion of the dependent variables in time, and then solved implicitly along with the interior point equations. Although points on the periodic lines and the branch cut are boundaries of the computational regime, they are interior flow fields points and must be treated as such. The present technique replaces derivatives at these points by central differences. In addition, in regard to the periodic lines the procedure inverts a matrix with strict periodic boundary conditions; i.e., the periodic line values are obtained from the implicit solution, rather than from an extrapolation or averaging procedure which uses interior computational grid point values.

This specification has worked very well when steady solutions are sought as convergence could be obtained very quickly. Using convergence

acceleration techniques described in Refs. 17 and 18 has allowed cascade calculations to converge very rapidly even for low Mach number subsonic flows which in general can be difficult to converge. A typical convergence history is presented in Fig. 18 which presents residual versus time step number for the subsonic cascade calculation corresponding to the experiment of Hobbs, et al (Ref. 16). As can be seen, the maximum residual in the flow field drops by three and one-half orders of magnitude in seventy time steps. The reason for the sudden jump at time sixty will be discussed shortly. The maximum residual is defined by the maximum imbalance of any equation at any point when the time-derivative terms are omitted. At seventy time steps the solution has essentially stopped changing and as shown in Fig. 19, the surface pressure calculated is in very good agreement with that measured. The reason for the jump in residual at time step 60 is the run protocol. The calculation was initiated with a moderate artificial dissipation which was dropped by an order of magnitude at time step 60.

Although these boundary conditions have proven effective and accurate in obtaining steady solutions, further assessment should be made when time-accurate solutions are sought. Application of boundary conditions has been an item of recent high interest (e.g. Ref. 19). These efforts have focused upon considerations such as the effect of boundary conditions upon convergence, proper boundary conditions for steady state solutions and proper boundary conditions for time-accurate solution. When the latter is sought, boundary conditions should not impose nonphysical wave reflections. Approaches focusing upon nonreflective boundary conditions have been formulated by several authors. For example, Bayliss and Turkel (Ref. 20) investigated boundary conditions which simulate correct radiation of energy outside of the computational domain. This approach requires the boundary condition to be a partial differential equation relating pressure, density and velocity. Applications for three-dimensional spherical radiation, two-dimensional radiation and one-dimensional radiation were considered. Rudy and Strikwerda (Ref. 21) also considered nonreflective boundary conditions and developed a specification which for their problem and numerical method hastened convergence to steady state, but did not attempt to maintain transient accuracy. Hedstrom (Ref. 22) considered nonreflective boundary conditions which maintained transient accuracy. Other approaches are given in Ref. 19. Based upon the discussions in Refs. 20-22, a

one-dimensional nonreflective boundary condition was added to the cascade code. This condition relates pressure and velocity by the equation

$$\frac{\partial p}{\partial t} - \rho c \frac{\partial q}{\partial t} = 0$$

where c is the speed of sound. The boundary condition was used in a calculation of the cascade of Ref. 16 and convergence was obtained although no significant improvement was found over the previous condition. However, this may be a more advantageous condition in transient flow situations.

The final item considered under the present year's effort focused upon choice of a stator-rotor grid. Two possibilities are immediately obvious. The first would use two distinct grids which overlap. One grid would be for the stator and one for the rotor. Each grid would be a 'C' or an 'O' grid such as those currently used at SRA. Under this procedure, the solution for the flow field about the stator would be marched through a time-step with the (matching plane) downstream boundary condition being set by the static pressure calculated for the rotor blade flow field at the required physical locations. Thereafter the solution for the rotor flow field would be marched one time step with the upstream boundary condition being set by the stator flow field total pressure results at the required location. Obviously, such a procedure requires the solution from one region to provide appropriate boundary conditions for the other. The major disadvantage associated with such an approach is the required lagging of boundary conditions and the interpolation to obtain boundary conditions. The interpolation as well as the lagged boundary conditions may adversely affect numerical stability and would reduce convergence rate even in stable calculations. Nevertheless, this may be a viable technique for the stator-rotor problem.

The second possible approach would use a single grid in which the stator would be embedded within a 'C' grid and the rotor within an 'H' grid. A sketch using a geometric configuration similar to that of Dring, et al (Ref. 5) is shown in Fig. 20. With this approach both rotor and stator flow fields are calculated as a unit with no need to interpolate or lag boundary conditions. Two problems arise with this approach. First, the rotor being embedded within an 'H' grid may exhibit poor behavior at the leading edge coordinate singularity, point A of Fig. 20. Secondly, as the gap between

blades is decreased the coordinate system will become increasingly nonorthogonal.

The first of these problems, the treatment of coordinate singular point, was investigated during the present reporting period through a sample calculation. In this calculation, flow about a Joukowski airfoil was considered with the computational grid being formed by the potential flow streamlines and potential lines. This grid is shown in Fig. 21. As can be seen, the grid is of an 'H' type, and has high resolution both in the leading edge region and in the region in the immediate vicinity of the airfoil.

The calculation was initiated from a uniform flow with an applied no-slip condition at the airfoil boundary. For the purpose of this calculation, the flow was assumed laminar with a Reynolds number based upon a chord of 1.5×10^5, and a free stream Mach number of .087. Convergence was obtained with no problem and no flow anomalies were noted in the vicinity of the leading edge. A comparison between calculated surface pressure distribution and that obtained analytically from potential flow theory is shown in Fig. 22. As can be seen, the agreement in the leading edge region is very good. The viscous results give a suction peak slightly less than the inviscid results. The major discrepancy is near midchord where separation occurs in the viscous laminar, calculations. This obviously changes the pressure distribution from that obtained via the potential flow analysis and the difference is as expected. Velocity vector plots are shown in Fig. 23, and static pressure contours in Fig. 24. The results obtained clarly indicate the ability of the present Navier-Stokes code to yield accurate results in the vicinity of the 'H'-grid coordinate singularity. Therefore, it appears that the 'H'-grid can be used for viscous calculations of the type anticipated.

The second problem concerns the gap spacing. According to Dring, et al (Ref. 5) axial rows in turbines contain gap spacing of 1/4 to 1/2 axial chord. Although conclusions must be tentative until demonstrated, it appears that this gap spacing range would not preclude the single grid approach.

PROFESSIONAL PERSONNEL ASSOCIATED WITH RESEARCH EFFORT

Stephen J. Shamroth

Henry McDonald

Bernard C. Weinberg

David V. Roscoe

John P. Kreskovsky

REFERENCES

1. Fleeter, S., Jay, R.L., and Bennett, W.A.: Compressor Stator Time-Variant Aerodyamic Response to Upstream Rotor Wakes, EDR 9005, Detroit Diesel Allison Contractor Report on Contract F44620-74-C-0065, November 1976.

2. Fleeter, S., Jay, R.L., and Bennett, W.A.: The Effect of Rotor-Stator Axial Spacing on the Time-Variant Aerodynamic Response of a Compressor Stator, EDR 9379, Detroit Diesel Allison Contractor report on Contract F49620-77-C-0024, December 1977.

3. Jay, R.L. and Bennett, W.A.: The Effects of Solidity, Interblade Phase Angle and Reduced Frequency on the Time-Variant Aerodynamic Response of a Compressor Stator, EDR 10339, Detroit Diesel Allison Contractor report on Contract F49620-78-C-0070, June 1980.

4. Jay, R.L. and Bettner, J.L.: Aerodynamically Induced Vibration, EDR 10840, Detroit Diesel Allison Contractor report on Contract F49620-80-C-0078, September 1981.

5. Dring, R.P., Joslyn, H.D., Hardin, L.W. and Wagner, J.H.: Turbine Rotor-Stator Interaction. ASME Paper 82-GT-3, 1982.

6. Shamroth, S.J., McDonald, H. and Briley, W.R.: Prediction of Cascade Flow Fields Using the Averaged Navier-Stokes Equations. ASME Journal of Engineering for Power, Vol. 106, 1984.

7. Shamroth, S.J. and McDonald, H.: Development of a Design-Oriented Navier-Stokes Analysis. Scientific Research Associates Report R84-910004-F, 1984.

8. Shamroth, S.J., Gibeling, H.J. and McDonald, H.: A Navier-Stokes Solution of Laminar and Turbulent Flow Through a Cascade of Airfoils. AIAA Paper No. 80-1426, 1980. (Also, SRA Report R79-920004-F, 1979.)

9. Shamroth, S.J., McDonald, H. and Briley, W.R.: Application of a Navier-Stokes Analysis to Transonic Cascade Flow Fields. ASME Paper 82-GT-235, 1982.

10. McDonald, H., Shamroth, S.J. and Briley, W.R.: Transonic Flows with Viscous Effects, Transonic Shock and Multi-Dimensional Flows: Advances in Scientific Computing. Academic Press, New York, 1982.

11. Shamroth, S.J.: A Navier-Stokes Calculation of the Airfoil Dynamic Stall Process. Paper presented at AFOSR/FSSRL/University of Colorado Workshop on Unsteady Separated Flow, August 1983.

12. St. Hilaire, A.O. and Carta, F.O.: Analysis of Unswept and Swept Wing Chordwise Pressure Data from an Oscillating NACA 0012 Airfoil Experiment, Vol. I - Technical Report, NASA CR-3567, 1983.

REFERENCES (Continued)

13. St. Hilaire, A.O. and Carta, F.O.: Analysis of Unswept and Swept Wing Chordwise Pressure Data from an Oscillating NACA 0012 Airfoil Experiment, Vol. II - Data Report, NASA CR-165927, 1983.

14. Giesing, J.P.: Nonlinear, Two-Dimensional Unsteady Potential Flow with Lift, AIAA Paper 66-968, 1966.

15. Briley, W.R. and McDonald, H.: Computation of Three-Dimensional Horseshoe Vortex Flow Using the Navier-Stokes Equations. Seventh International Conference on Numerical Methods in Fluid Dynamics, 1980.

16. Hobbs, D.E., Wagner, J.H., Dannenhoffer, J.F., Dring, R.P.: Wake Experiment and Modelling for Fore and Aft-loaded Compressor Cascade. Pratt and Whitney Aircraft Report FR13514, 1980.

17. Briley, W.R., McDonald, H. and Shamroth, S.J.: A Low Mach Number Euler Formulation and Application to Time Iterative LBI Schemes. AIAA Journal, Vol. 21, 1983.

18. Briley, W.R. and McDonald, H.: Computational Fluid Dynamic Aspects of Internal Flow. AIAA Paper 79-1455, 1979.

19. Numerical Boundary Condition Procedures. NASA CP2201, 1981.

20. Bayliss, A. and Turkel, E.: Far Field Boundary Conditions for Compressible Flow, NASA CP2201, 1981.

21. Rudy, D.H. and Strikwerda, J.C.: A Nonreflecting Outflow Boundary Condition for Subsonic Navier-Stokes Equations, Journal of Computational Physics, Vol. 36, 1980.

22. Hedstrom, G.W.: Nonreflecting Boundary Conditions for Nonlinear Hyperbolic Systems, Journal of Computational Physics, Vol. 30, 1979.

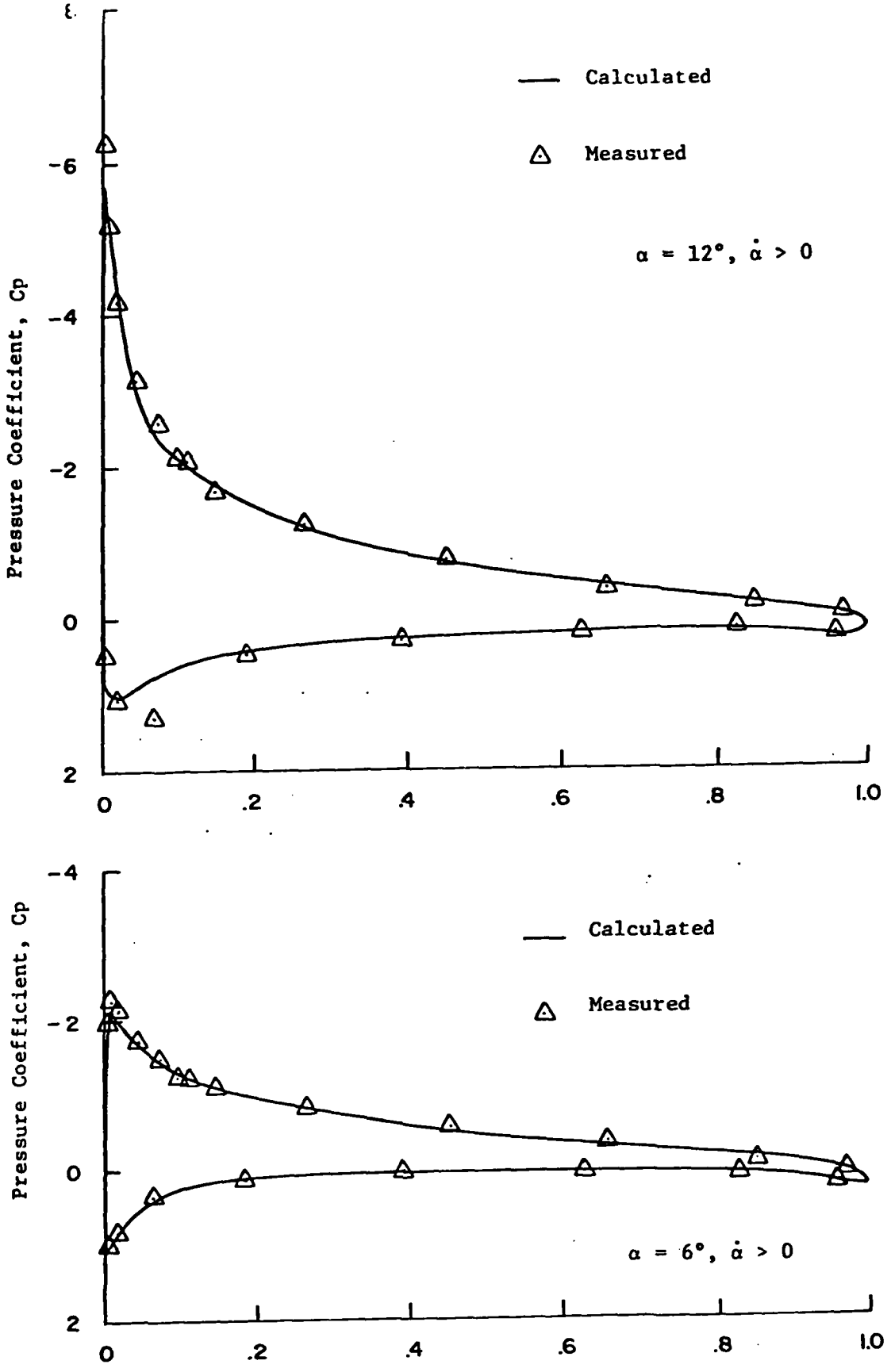

Fig. 1 - Pressure coefficient comparison - NACA 0012 airfoil.
$\alpha = 6°, 12°, \dot{\alpha} > 0$

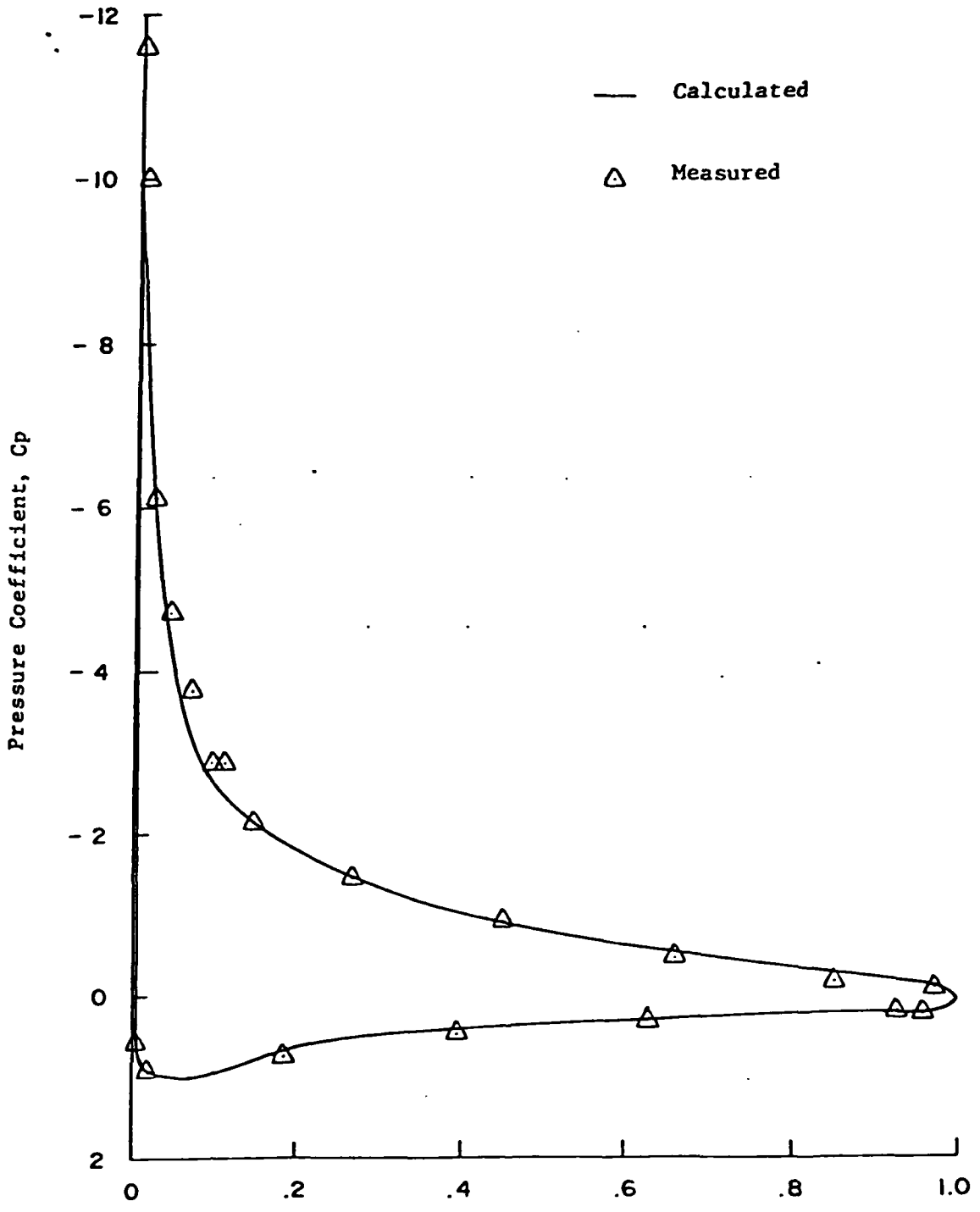

Fig. 2 - Pressure coefficient comparison - NACA 0012 airfoil.
$\alpha = 15.9°$, $\dot{\alpha} > 0$

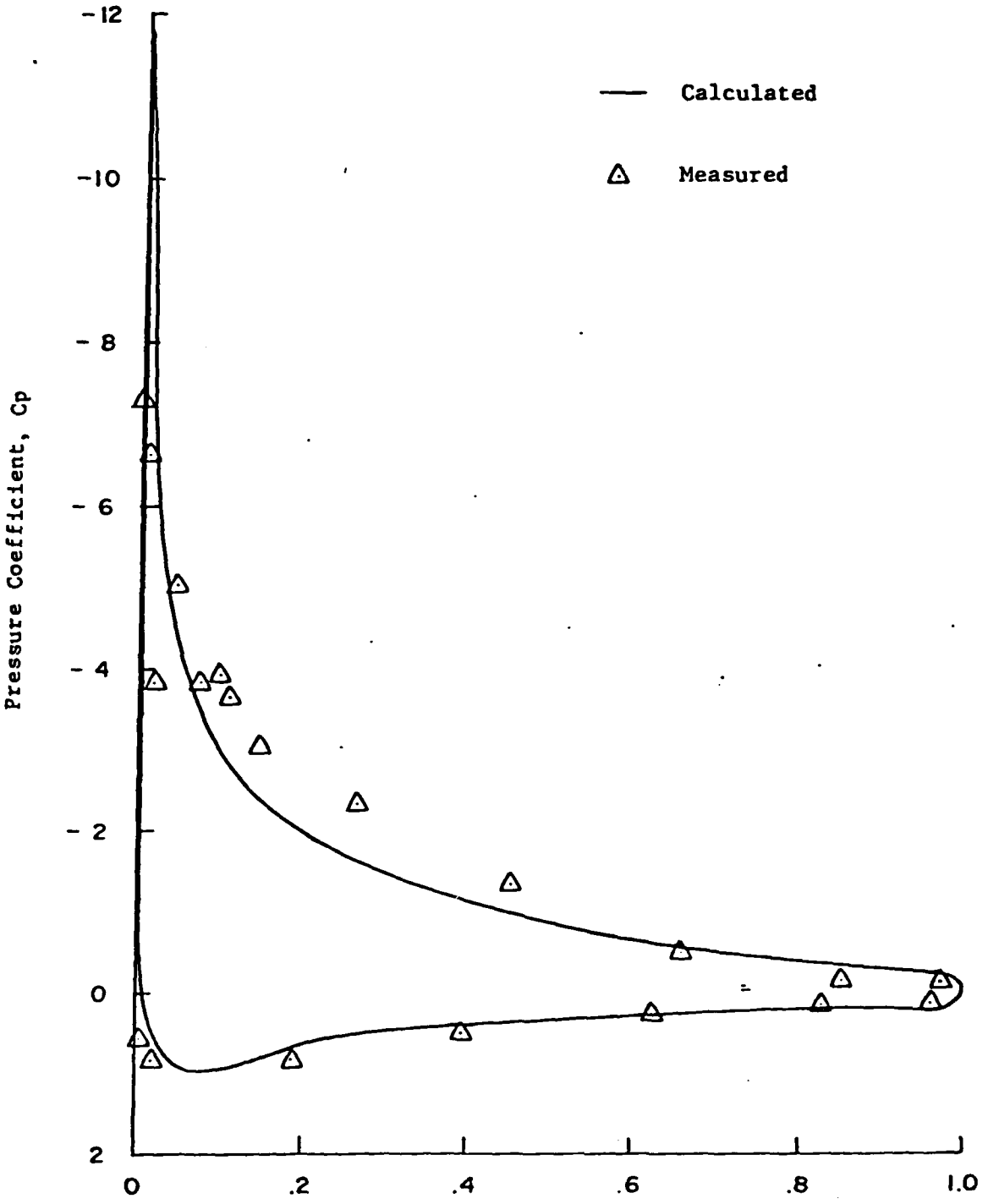

Fig. 3 - Pressure coefficient comparison - NACA 0012 airfoil.
$\alpha = 17.7°$, $\dot{\alpha} > 0$

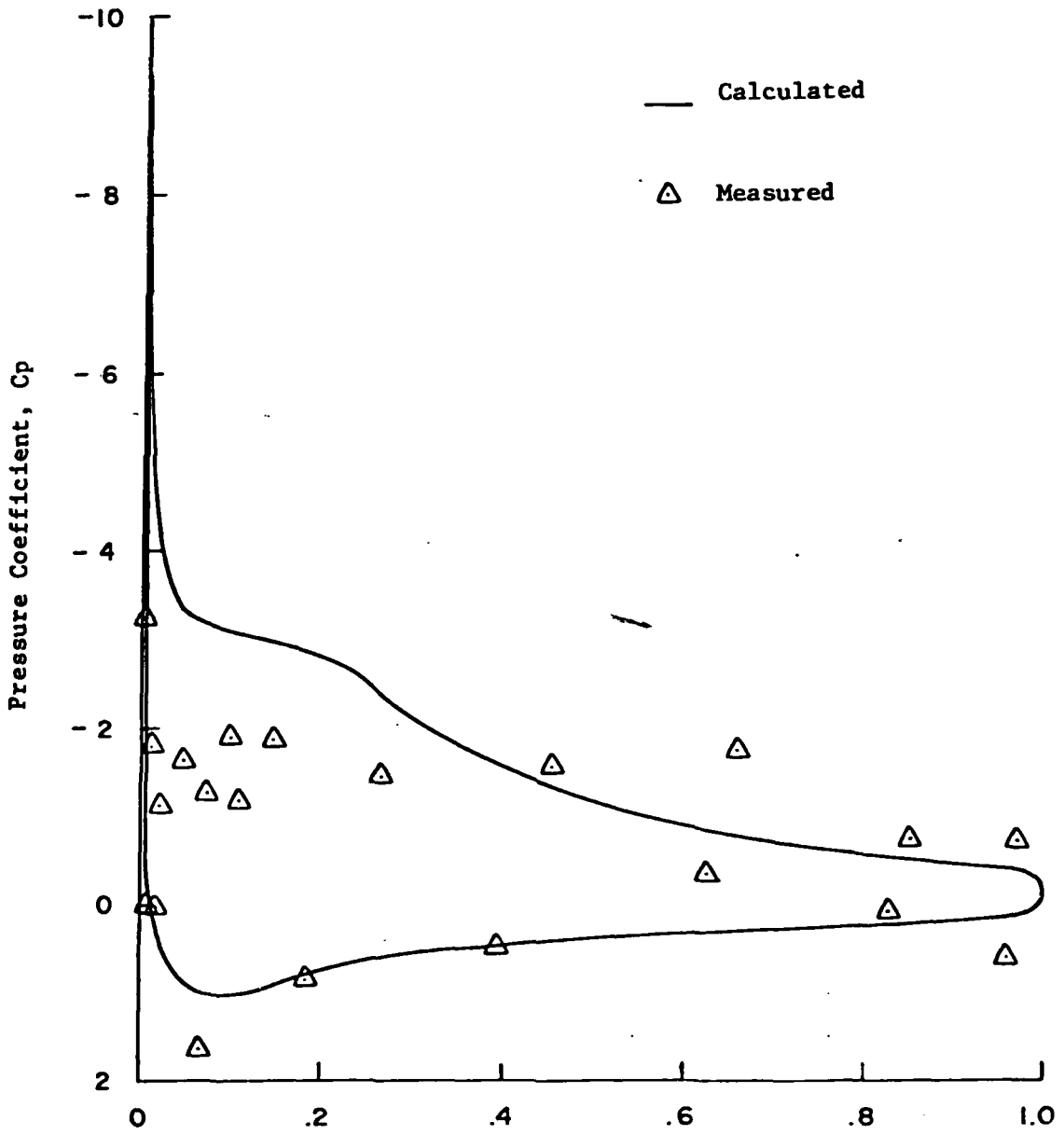

Fig. 4 - Pressure coefficient comparison - NACA 0012 airfoil. $\alpha = 19.5°$, $\dot{\alpha} > 0$

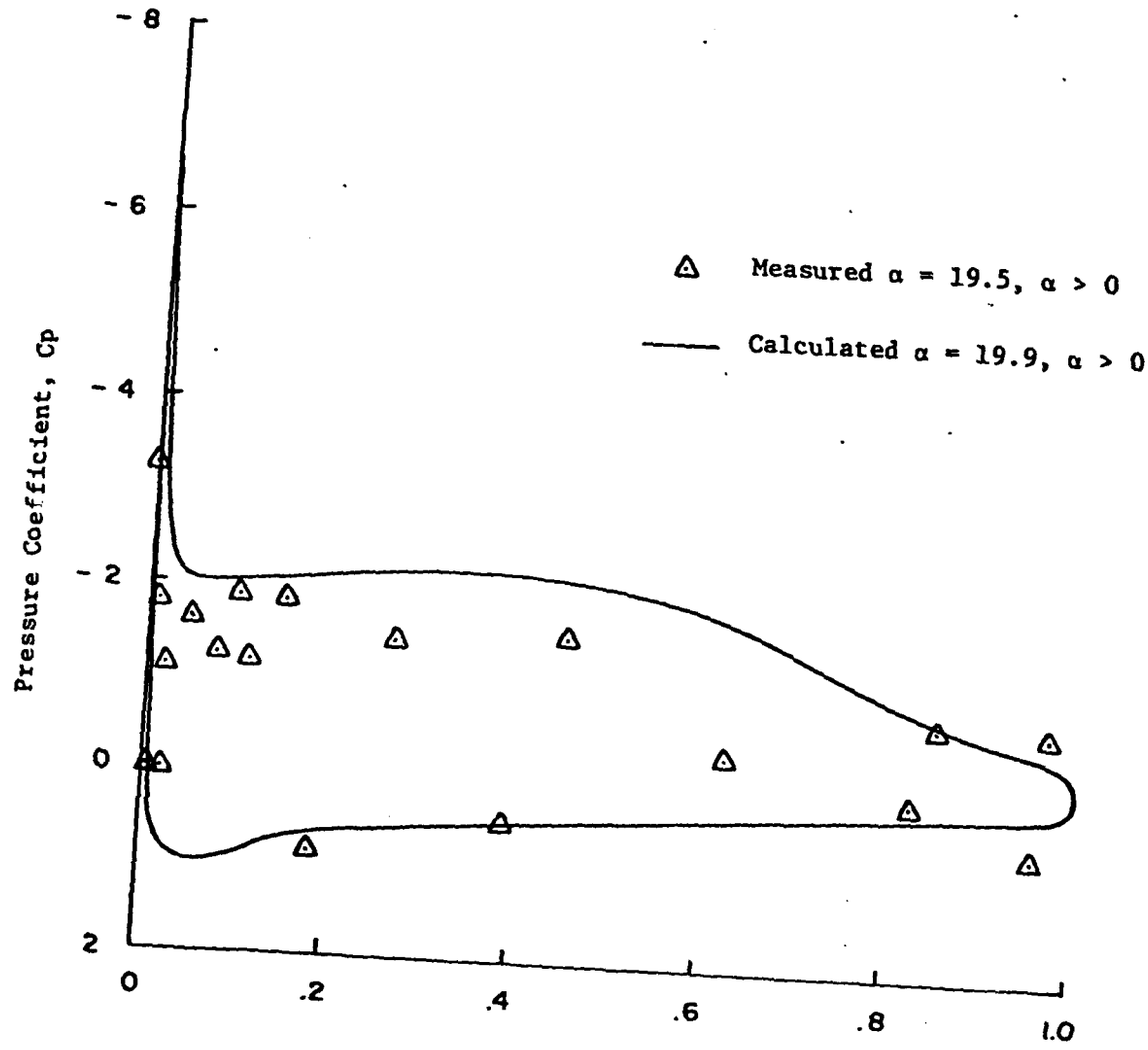

Fig. 5 - Pressure coefficient comparisons - NACA 0012 airfoil.

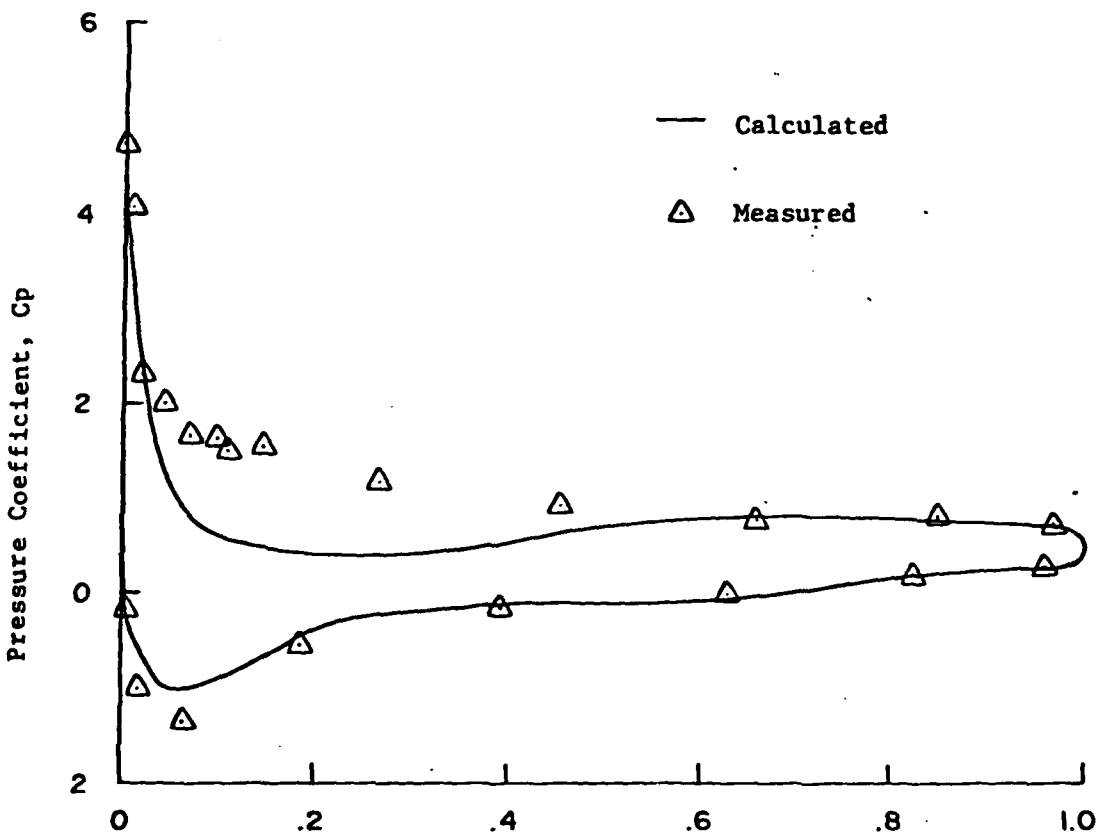

Fig. 6 - Pressure coefficient comparison - NACA 0012 airfoil. $\alpha = 18.3°$, $\dot{\alpha} < 0$

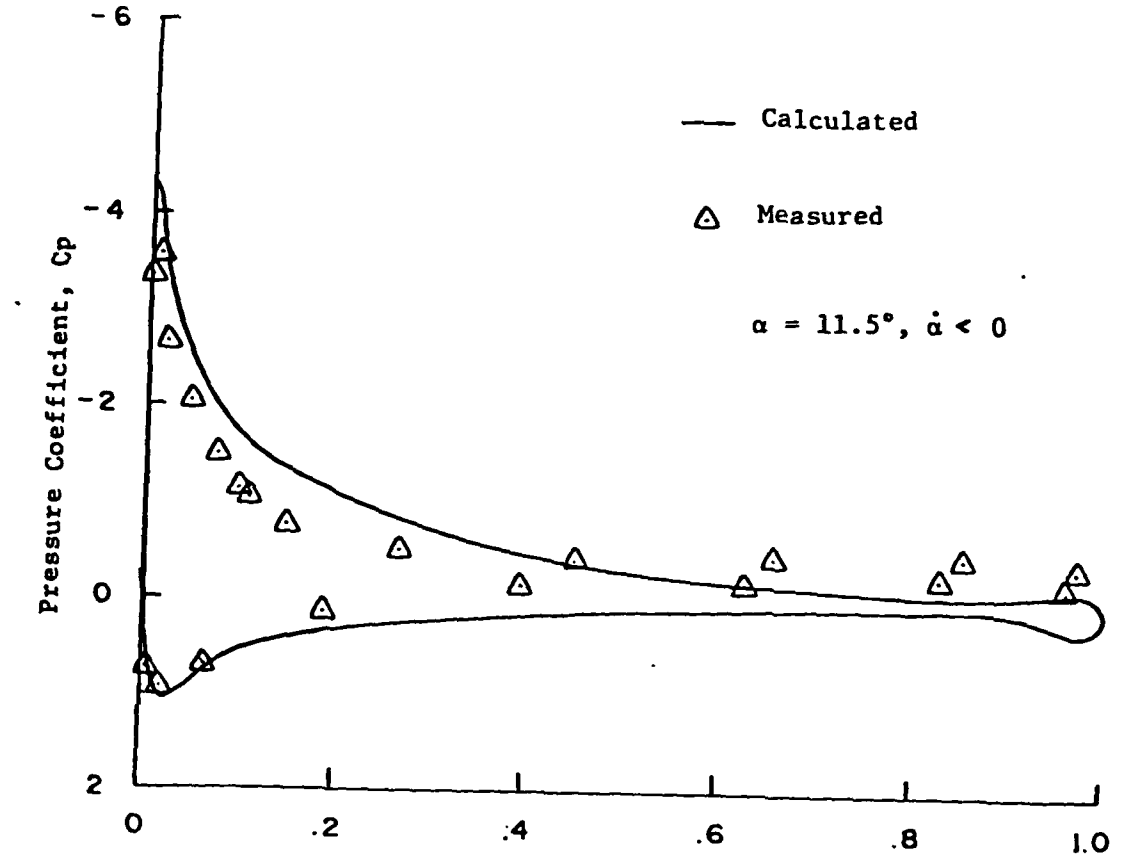

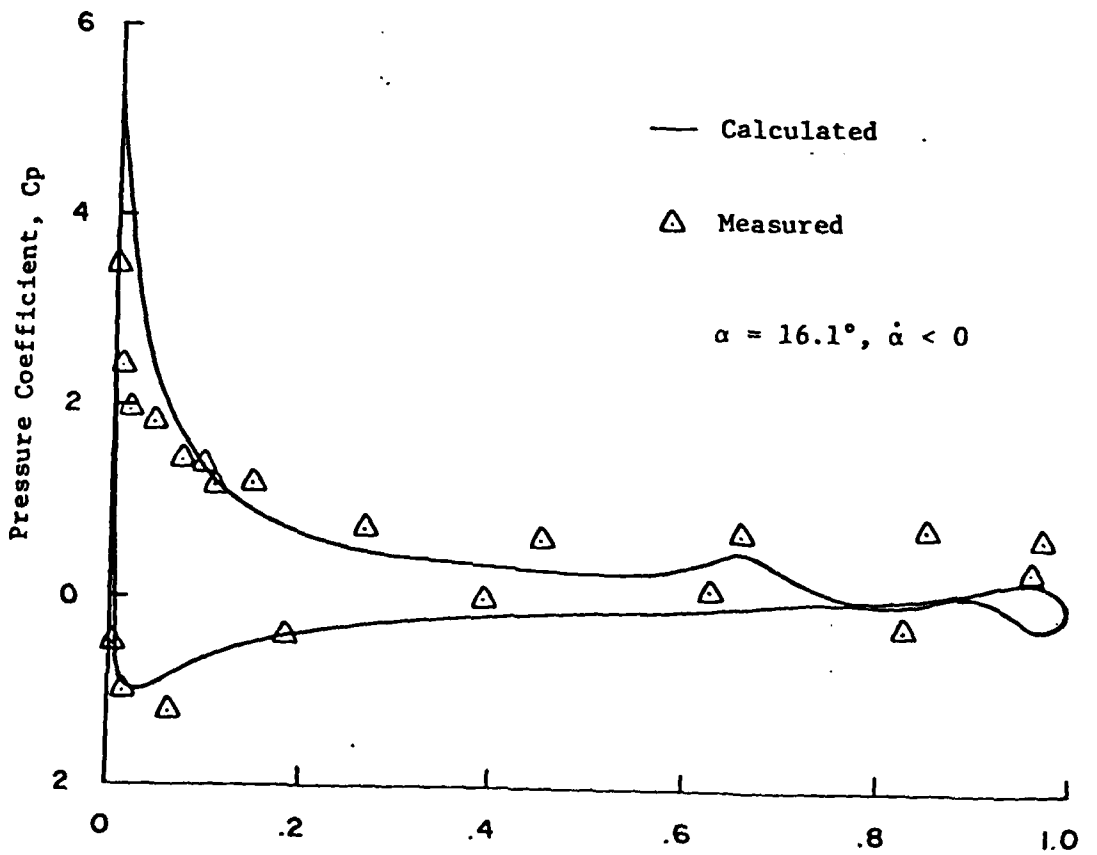

Fig. 7 - Pressure coefficient comparison - NACA 0012 airfoil.

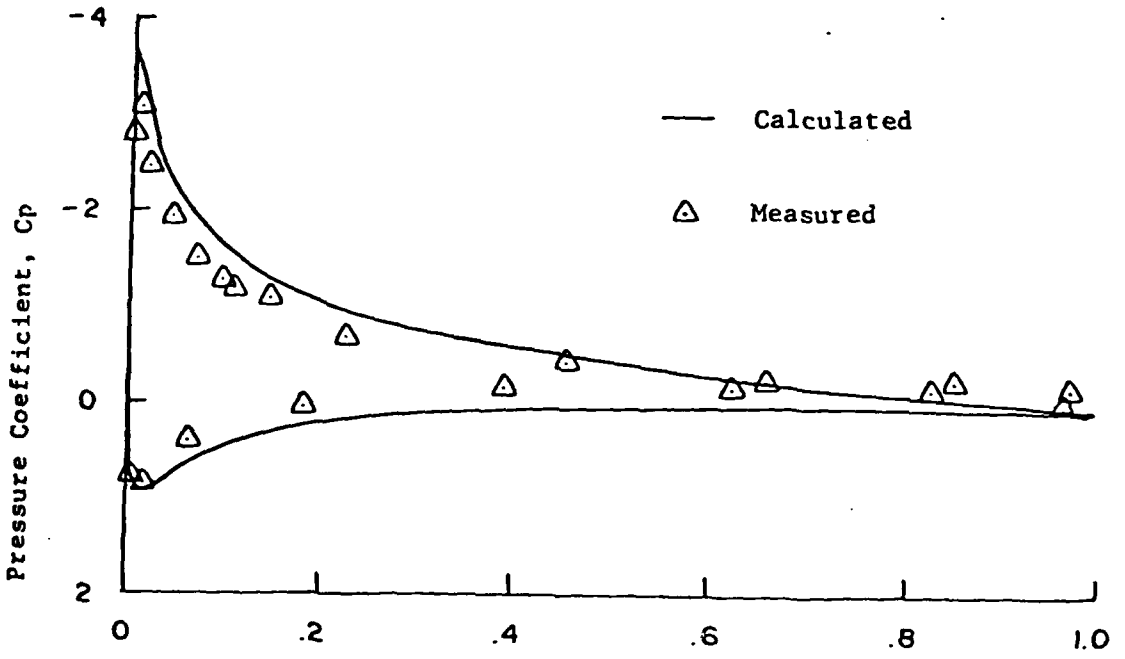

Fig. 8 - Pressure coefficient comparison - NACA 0012 airfoil. $\alpha = 8.5°$, $\dot{\alpha} < 0$

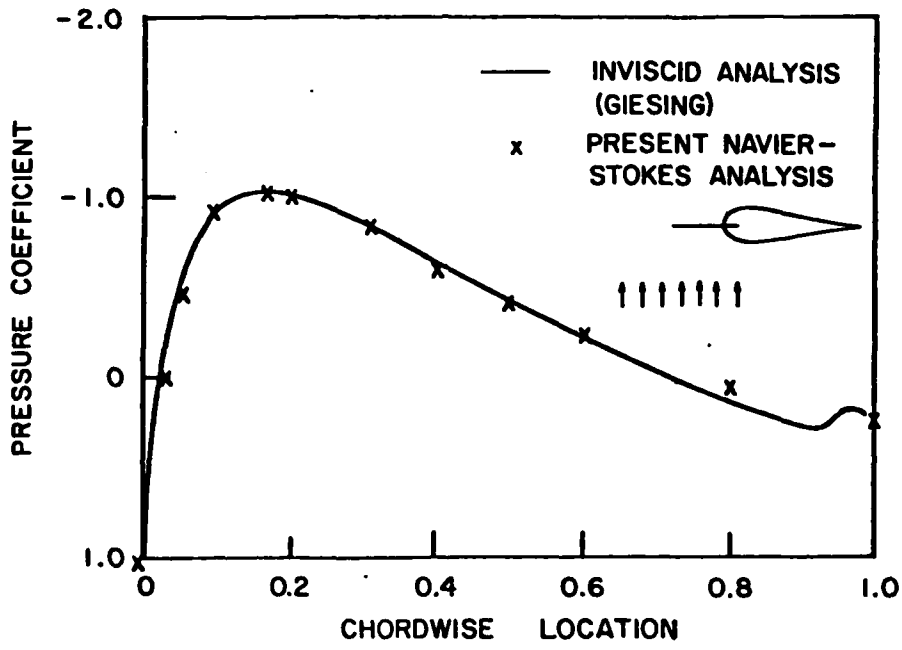

FIGURE 9. PRESSURE COEFFICIENT FOR 0.255 THICK JOUKOWSKI AIRFOIL ENTERING GUST, $T = -\infty$

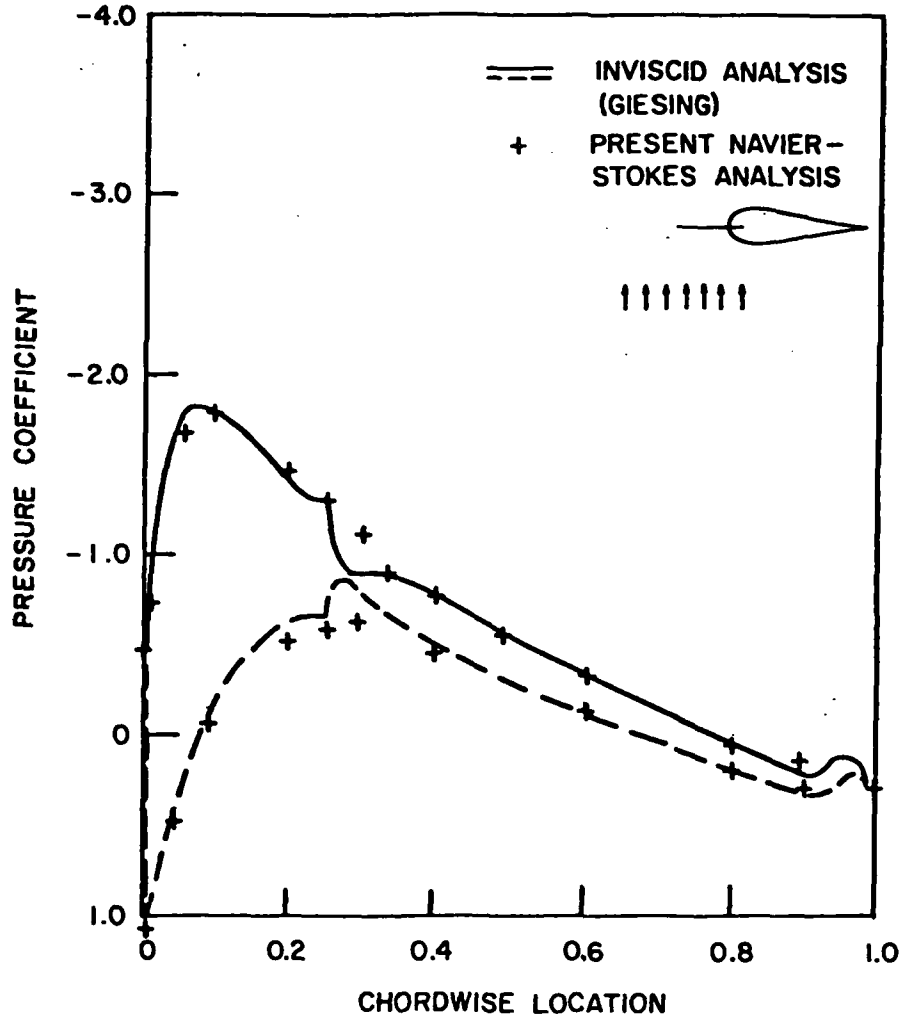

FIGURE 10. PRESSURE COEFFICIENT FOR 0.255 THICK JOUKOWSKI AIRFOIL ENTERING GUST, T = 0.25

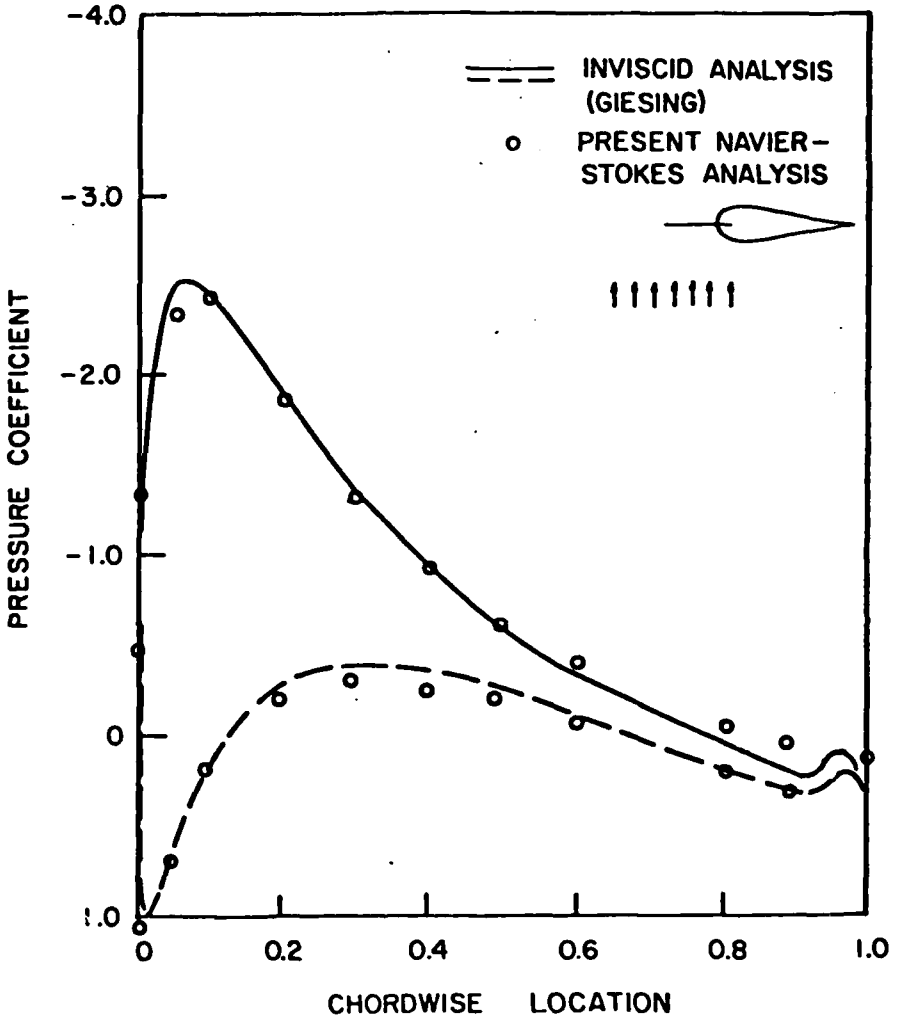

FIGURE 11. PRESSURE COEFFICIENT FOR 0.255 THICK JOUKOWSKI AIRFOIL ENTERING GUST, T = 1.00

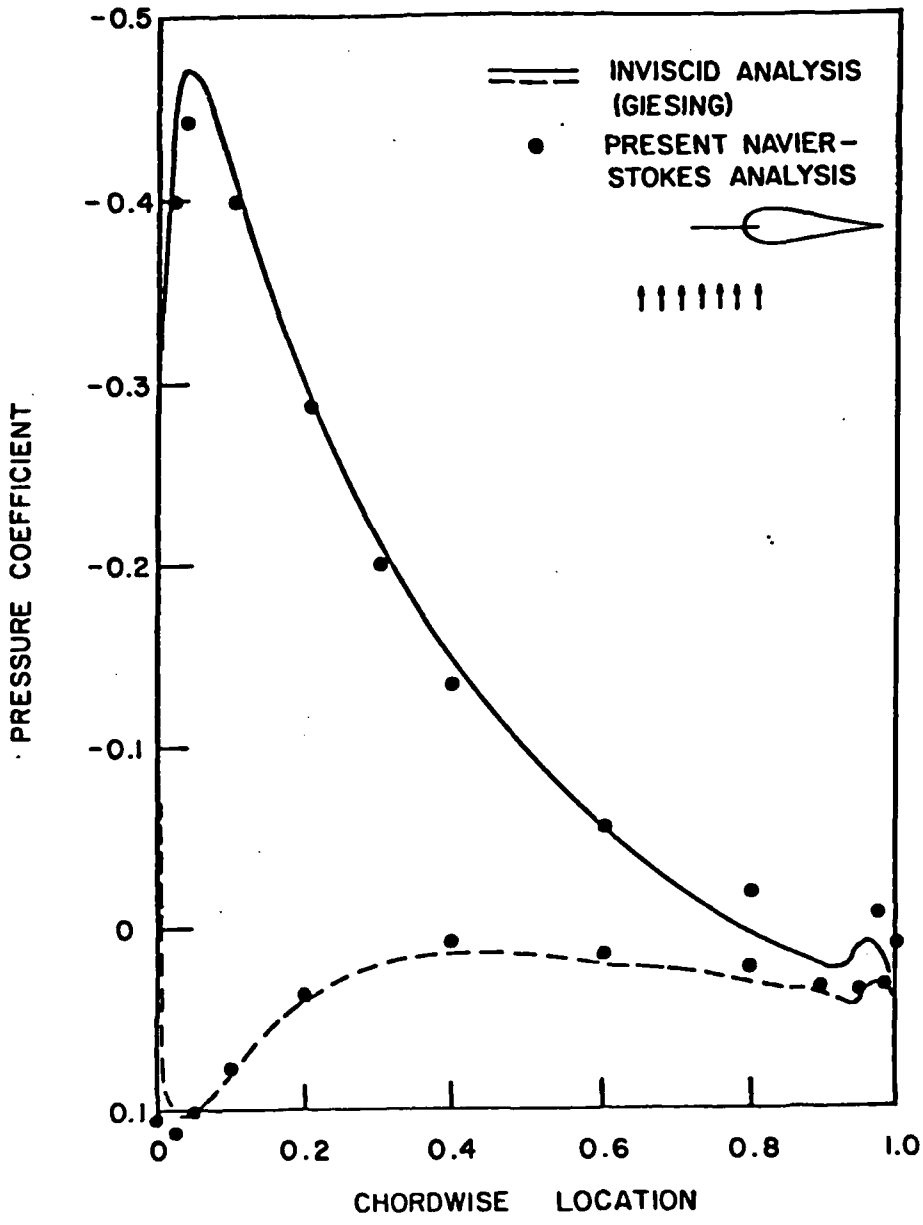

FIGURE 12. PRESSURE COEFFICIENT FOR 0.255 THICK JOUKOWSKI AIRFOIL ENTERING GUST, $T = \infty$

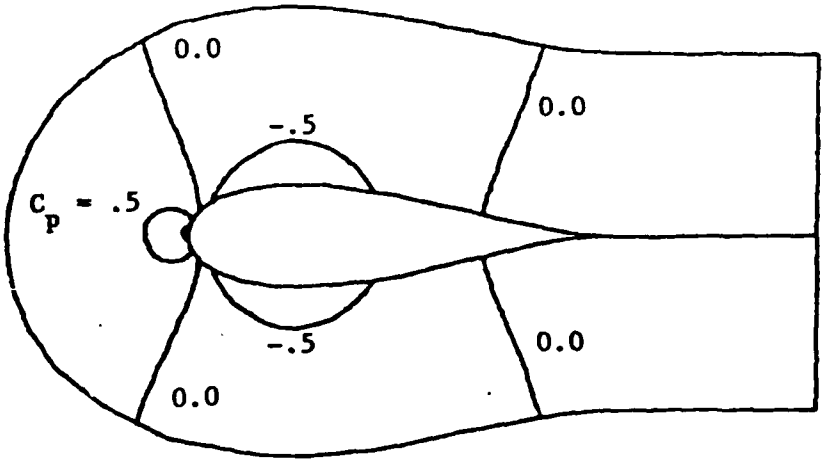

T = - .8

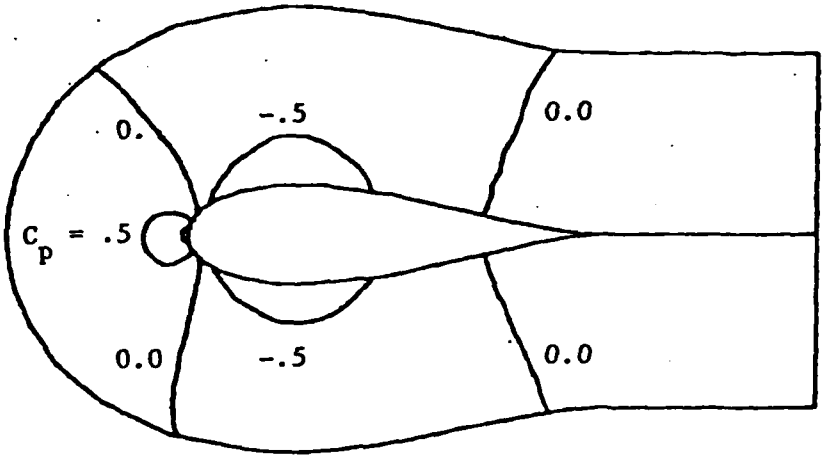

T = - .6

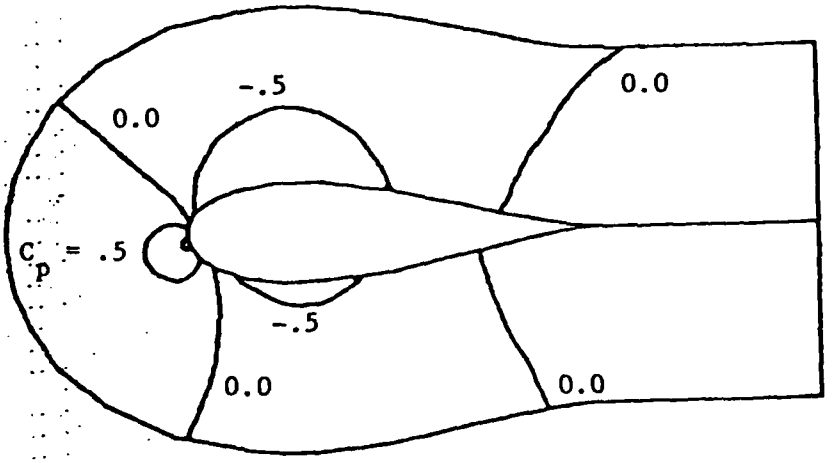

T = - .10

Fig. 13 - Pressure coefficient contour plot, Joukowski .255 airfoil in gust.

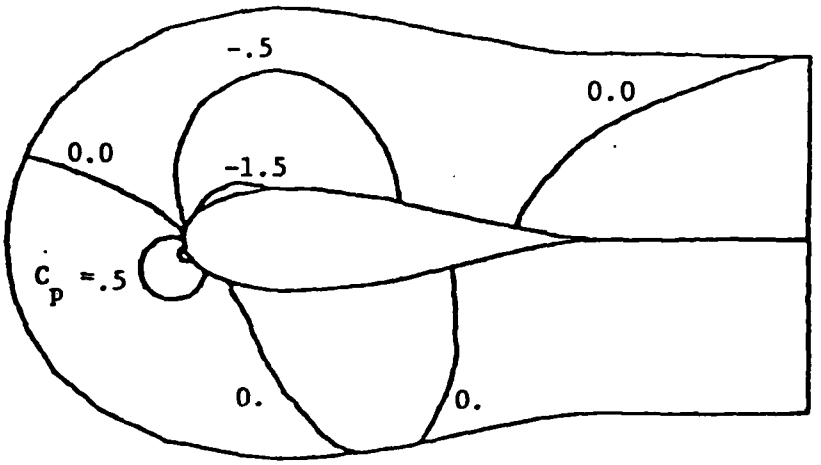

T = .23

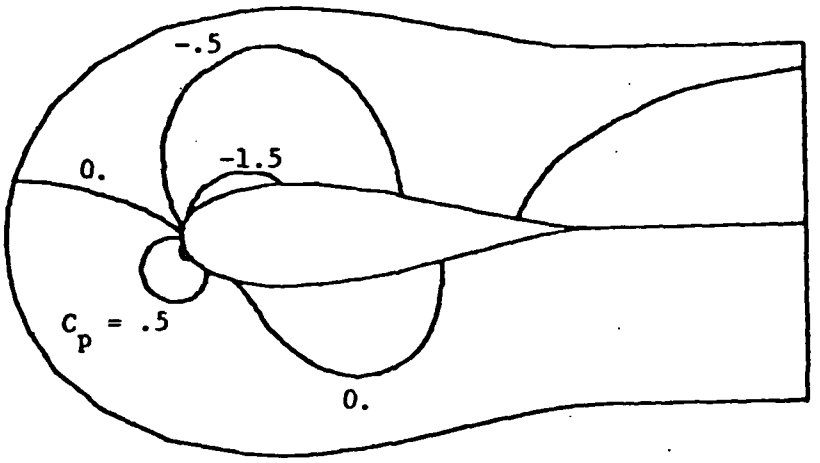

T = .70

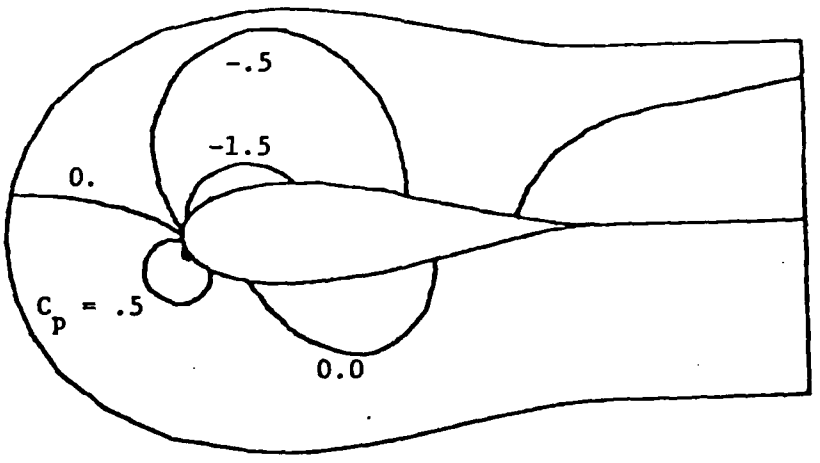

T = 1.10

Fig. 14 - Pressure coefficient contour plot, Joukowski .255 thick airfoil in gust.

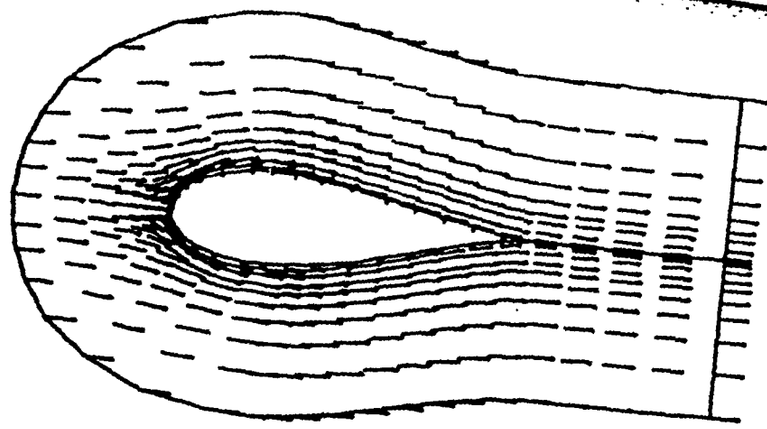

T = - .8

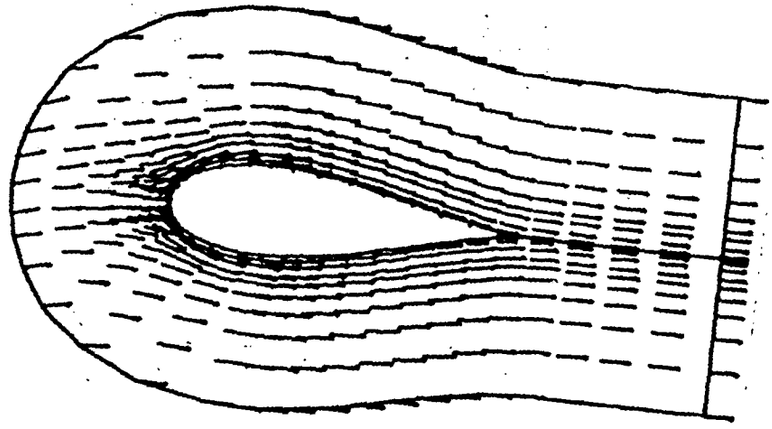

T = - .6

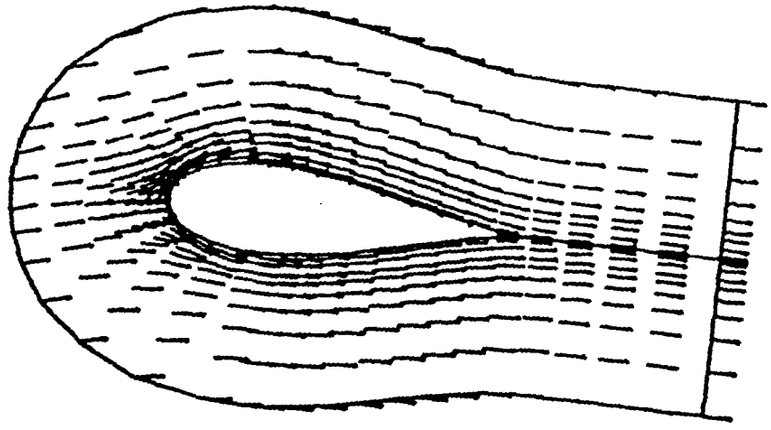

T = - .10

Fig. 15 - Vector plot, Joukowski .255 thick airfoil in gust.

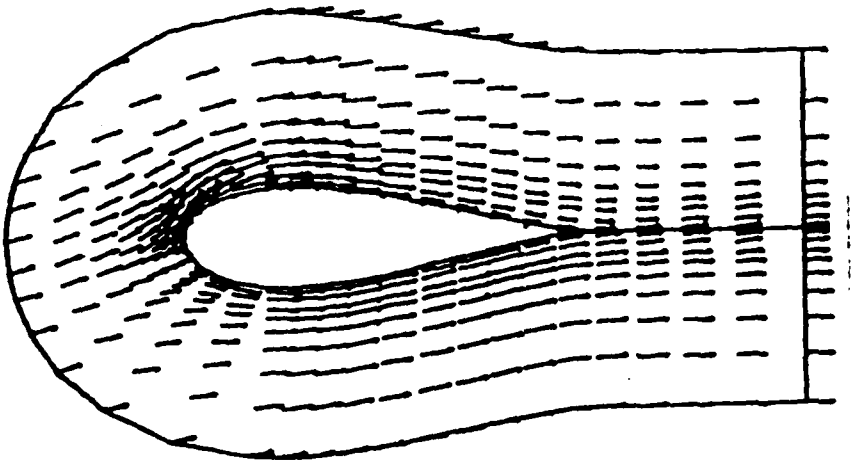

T = .23

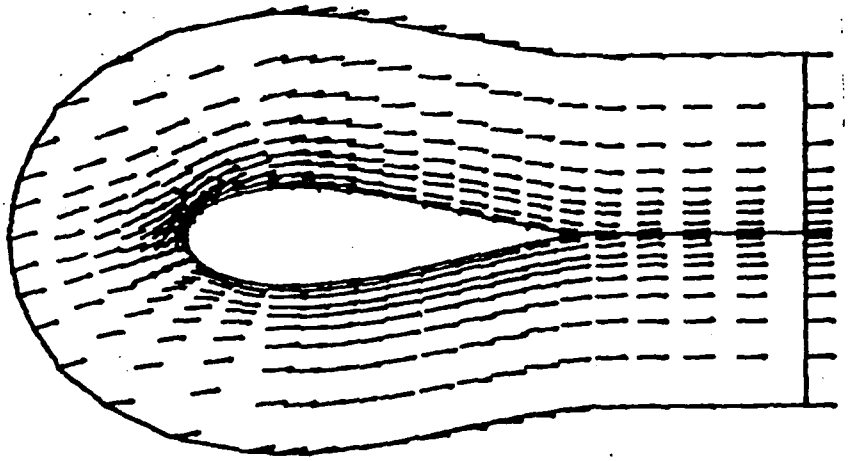

T = .70

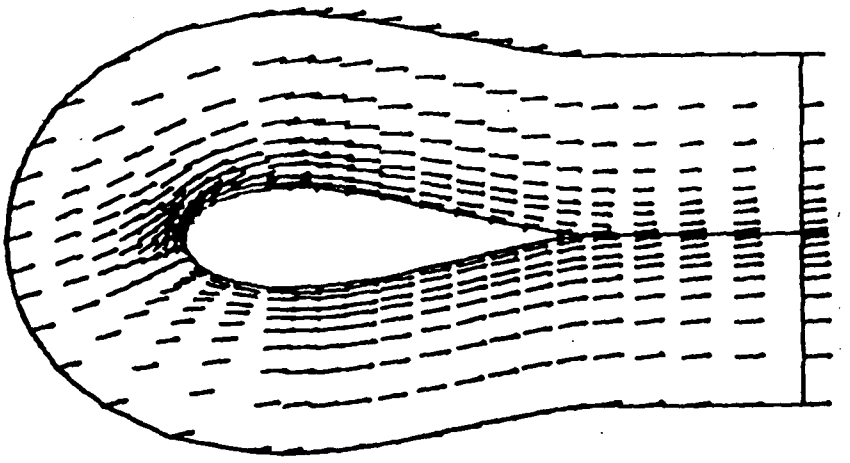

T = 1.10

Fig. 16 - Vector plot, Joukowski .255 thick airfoil in gust.

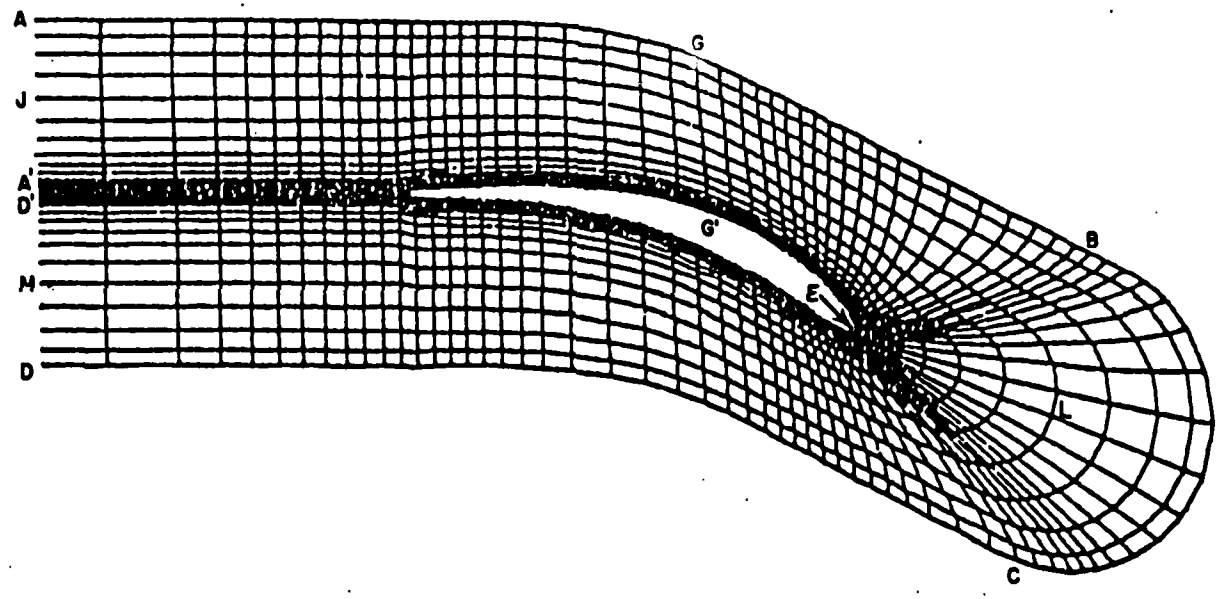

Fig. 17 - Constructive coordinate system.

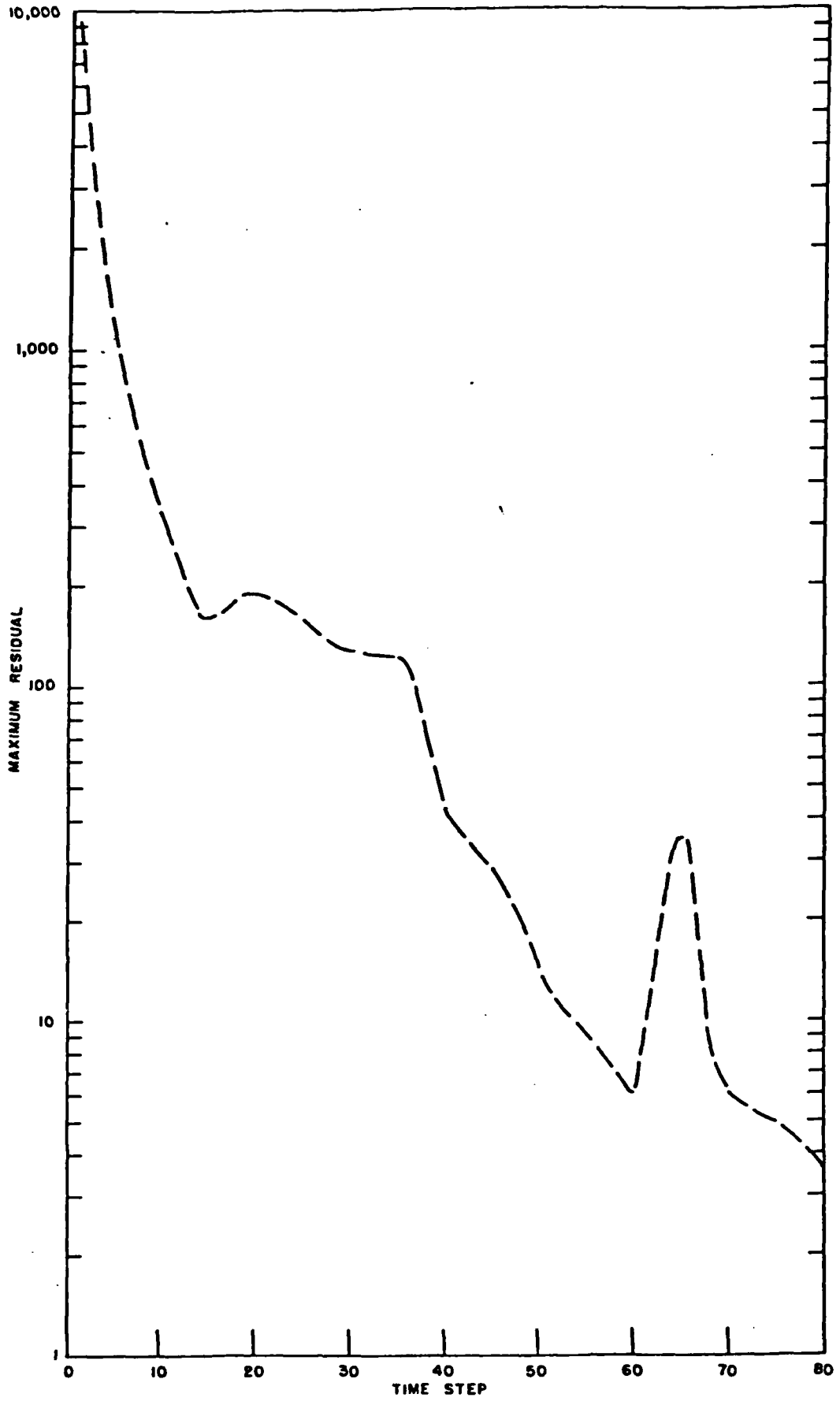

Fig. 18 - Iteration history, Hobbs subsonic cascade.

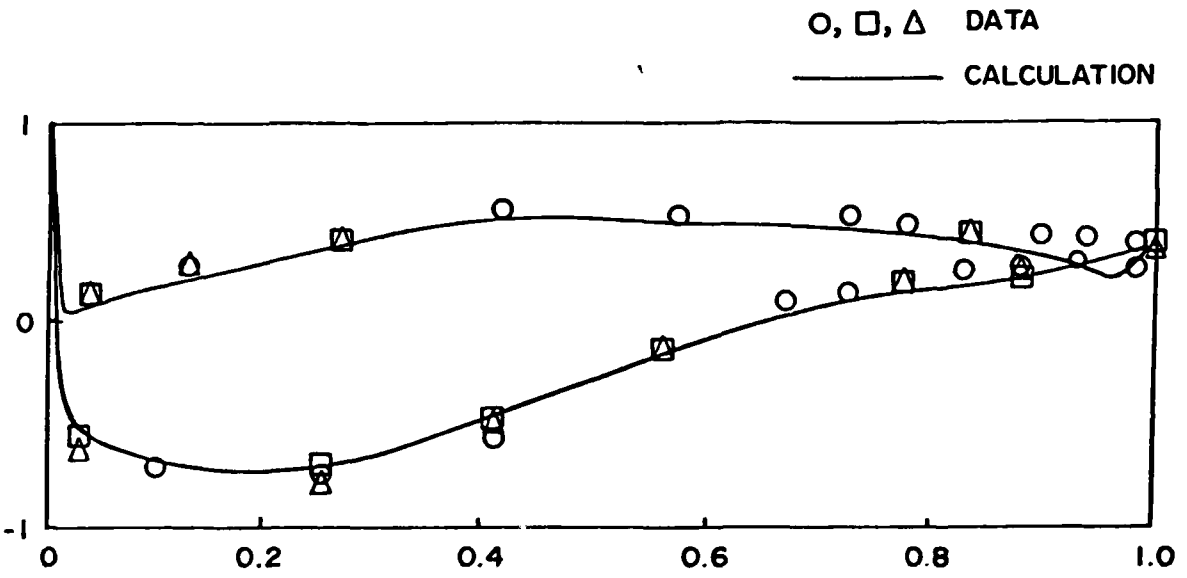

Fig. 19 - Calculated and measured pressure distribution, subsonic compressor cascade.

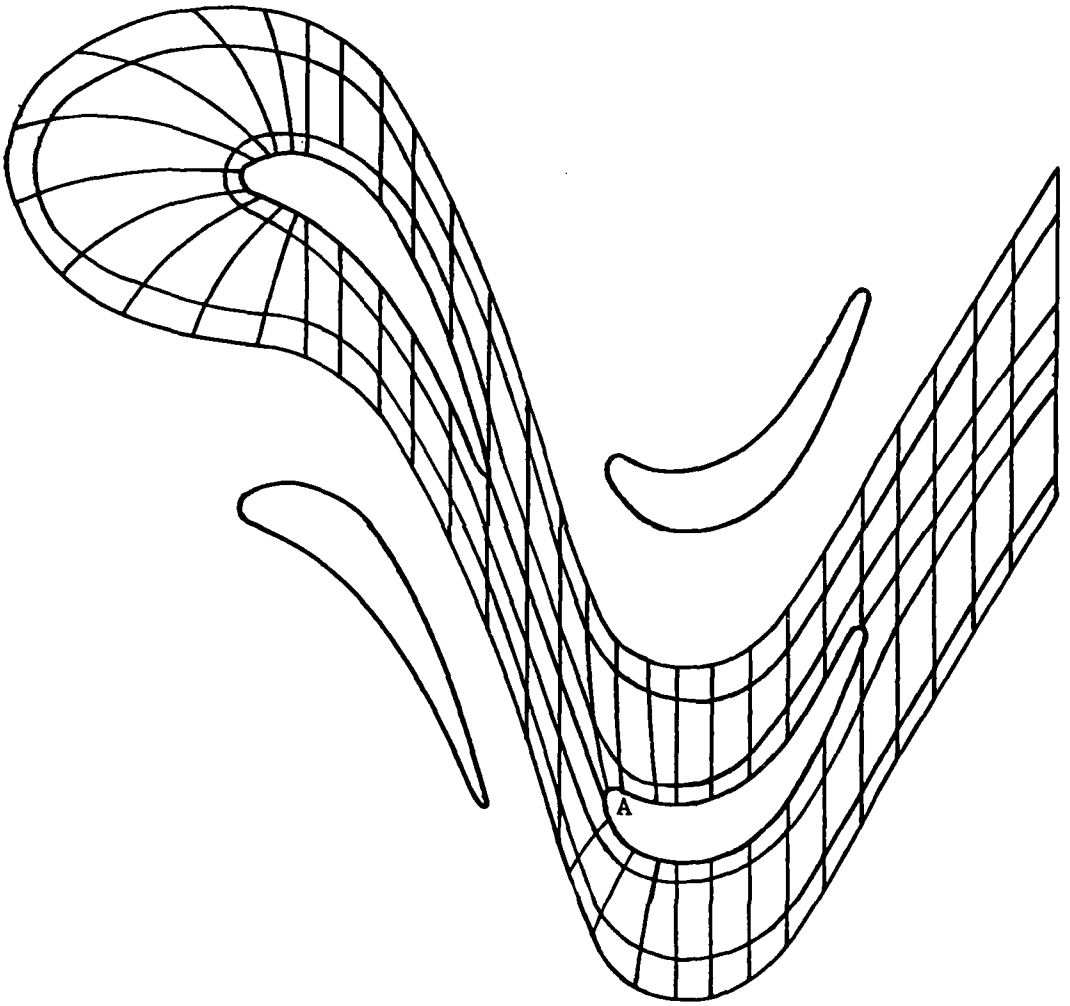

Fig. 20 - Sketch of proposed computational grid.

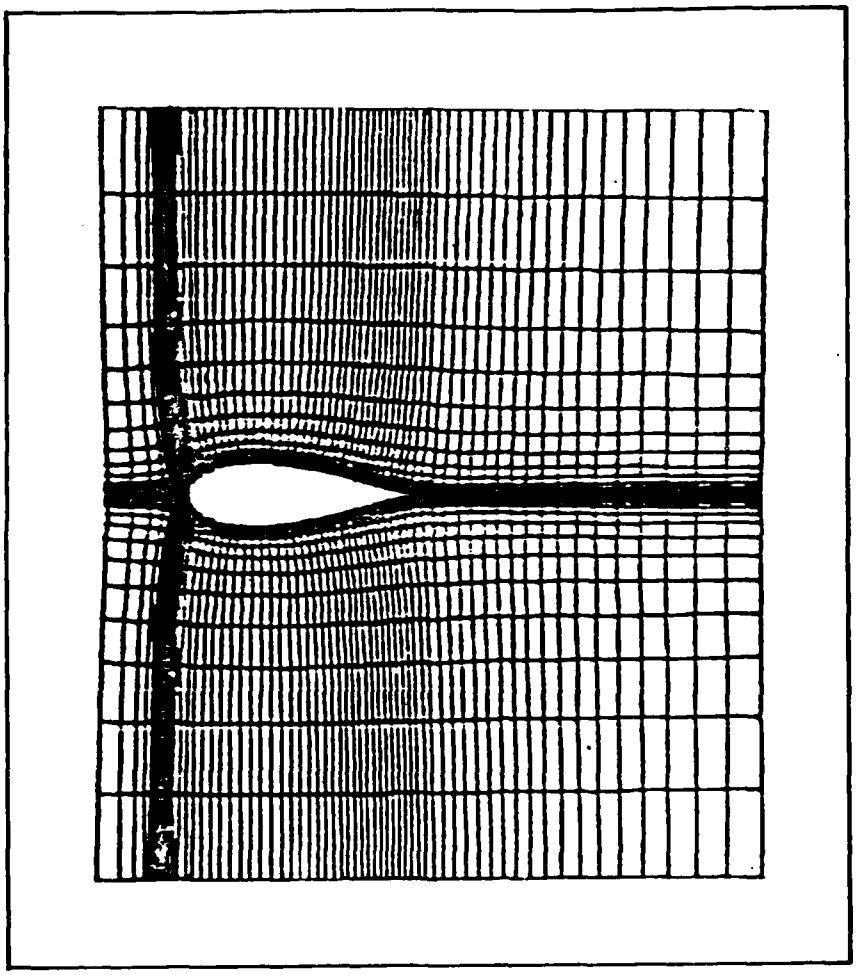

Fig. 21 - H-Grid coordinate system in the vicinity of the Joukowski airfoil.

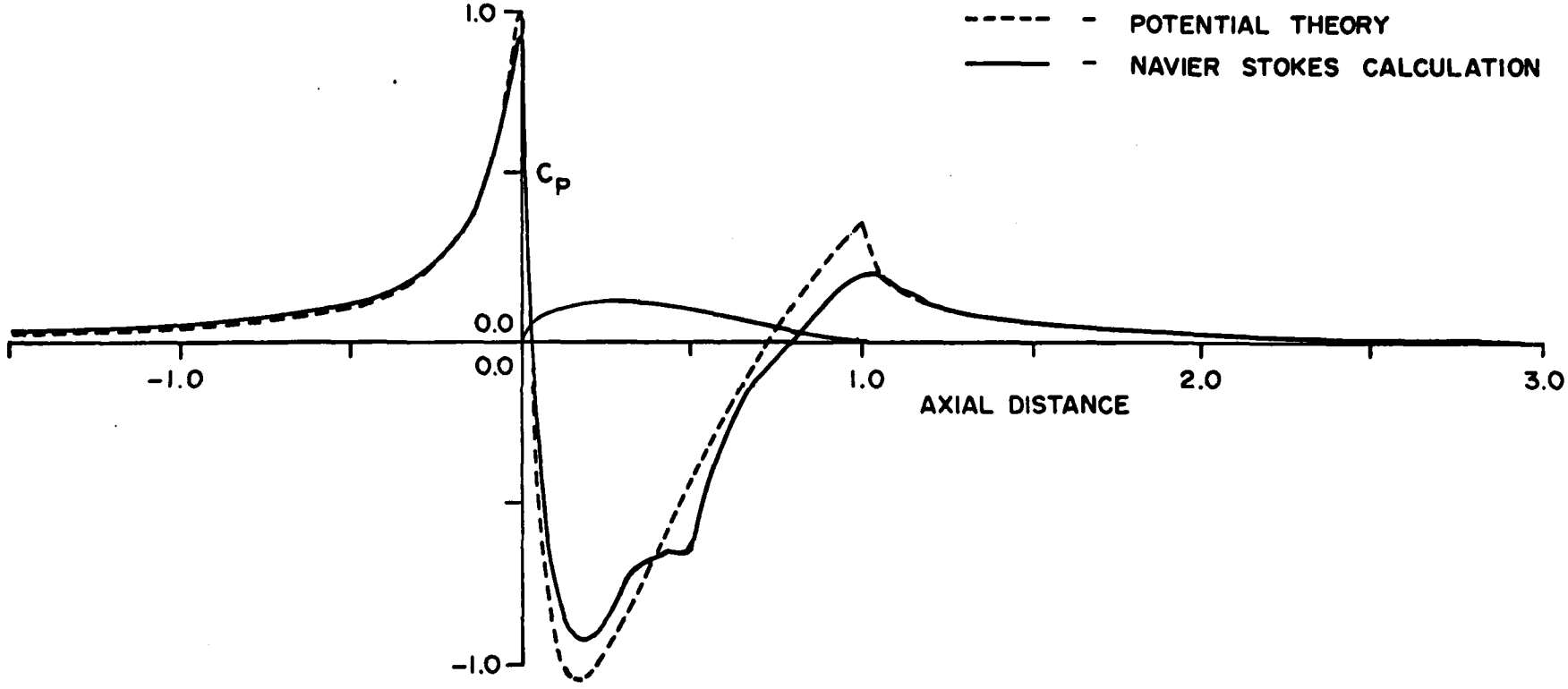

Fig. 22 - Surface pressure coefficient distribution about Joukowski airfoil.

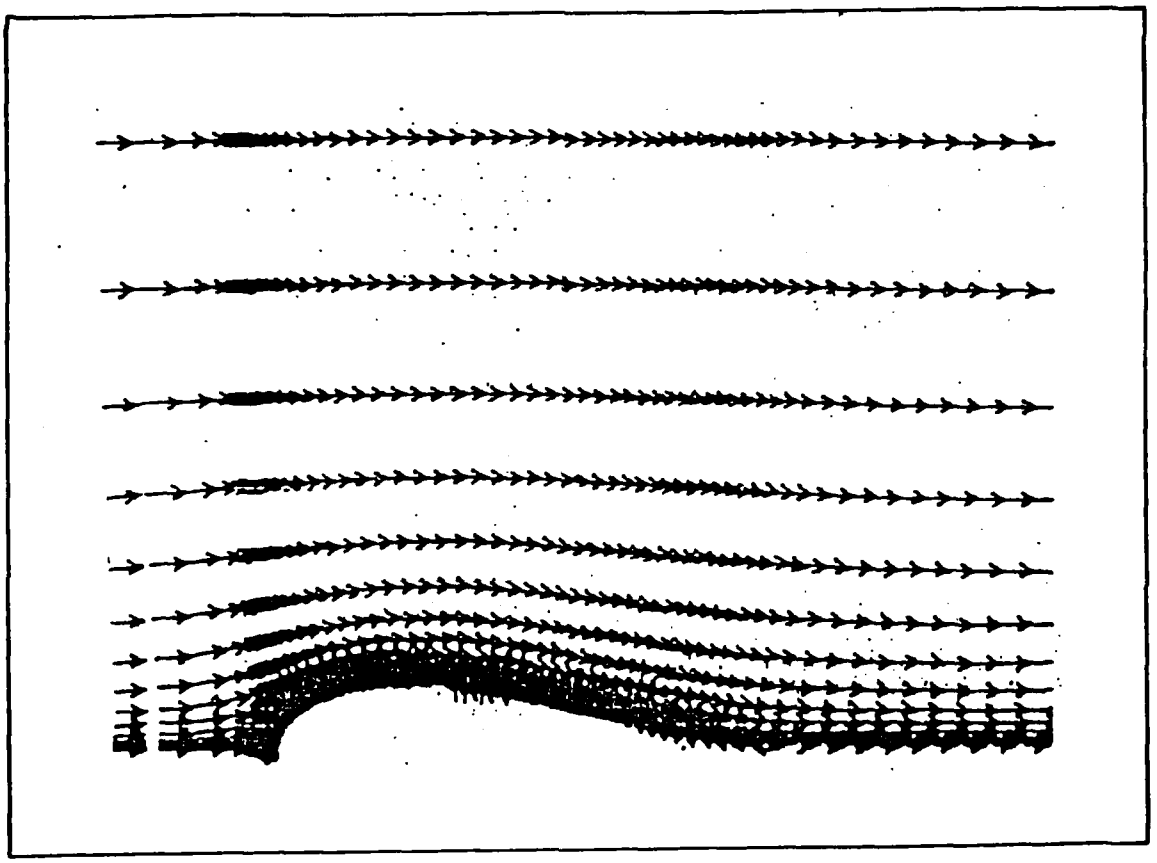

Fig. 23 - Velocity vector distribution on top surface of airfoil.

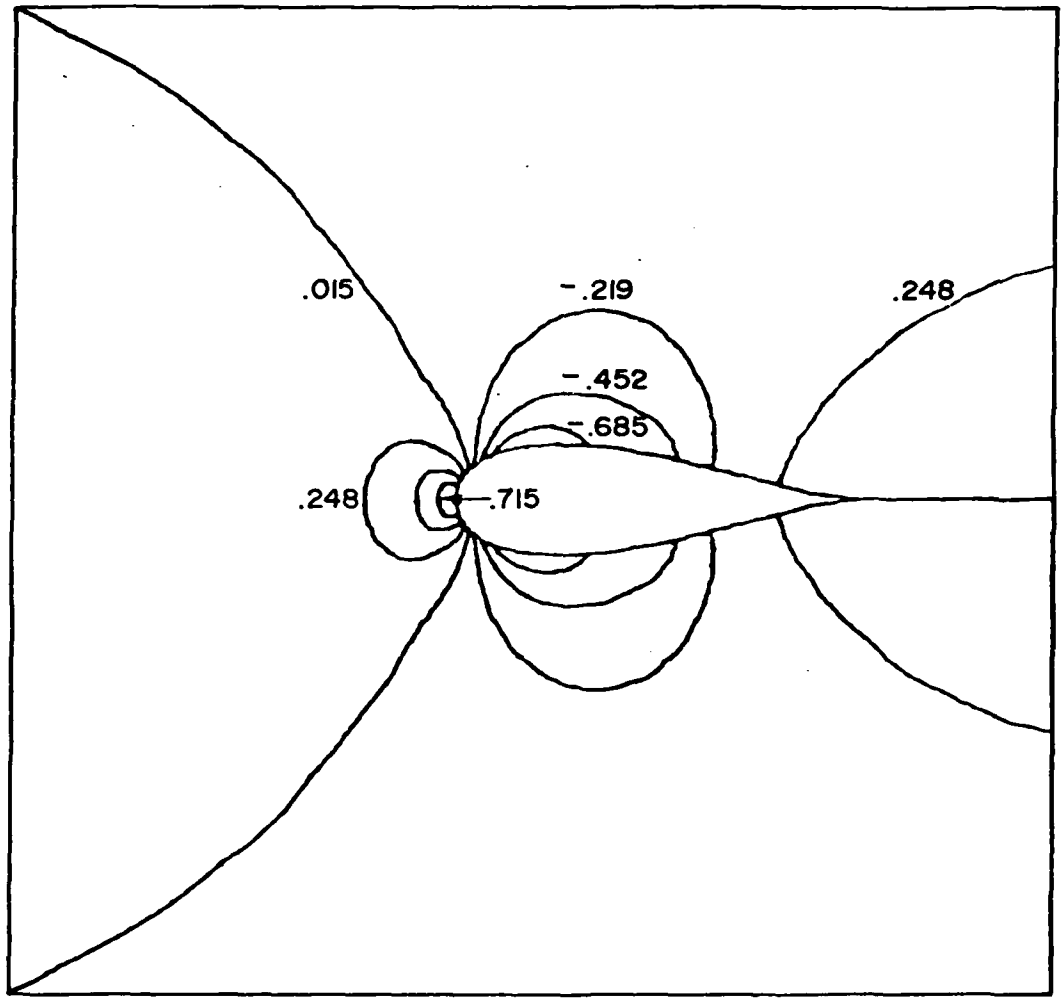

Fig. 24 - Pressure coefficient distribution about Joukowski airfoil.

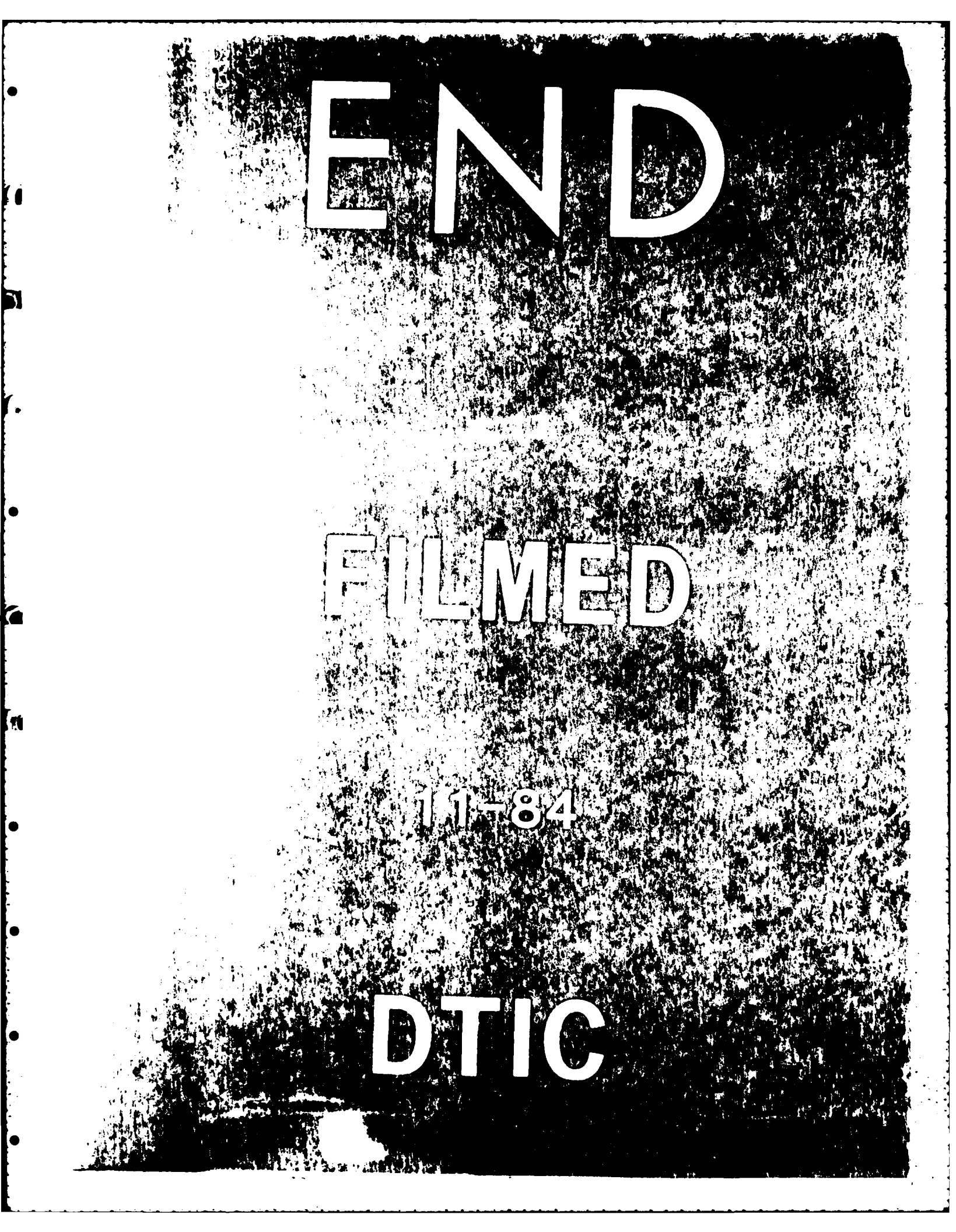
END
FILMED
11-84
DTIC